ACS EARTH AND SPACE CHEMISTRY

http://pubs.acs.org/journal/aesccq

Article

Differences between Laminated and Massive Shales in the Permian Lucaogou Formation: Insights into the Paleoenvironment, Petrology, Organic Matter, and Microstructure

Guangqing Yang, Jianhui Zeng,* Juncheng Qiao,* Yazhou Liu, Weifu Cao, Chengyun Wang, Feng Geng, and Wenfei Wei

Cite This: *ACS Earth Space Chem.* 2022, 6, 2530−2551

Read Online

ACCESS | Metrics & More | Article Recommendations

ABSTRACT: The Permian Lucaogou Formation (LCG Fm.) in the Junggar Basin is an organic-rich source rock interval formed in a salinized paleolake, and organic-rich laminated and massive shales are broadly deposited. However, the paleoenvironment difference between laminated and massive shales is still unclear, and the effect of this difference on petrology, pore structure, and organic matter enrichment is significant to shale oil resource evaluation. In this study, organic and element geochemistry, mineralogy, and nitrogen adsorption are used to analyze key differences between laminated and massive shales. The results show that most shale samples present mature thermal stage and oil-prone type II kerogen. Felsic igneous rocks in the continental island arc are their primary mineral component sources. The differences between laminated and massive shales are mainly from their silica origin, paleoclimate, and salinity. The silica origin in laminated shale is primarily from the terrestrial debris influx, while the massive shale is mixed with terrestrial debris and biogenic origin. The silica origin from hydrothermal activities is negligible. The laminated shale prefers to be deposited in a hot and dry climate with weak weathering and relatively higher salinity. However, the massive shale is mainly deposited in a warm and humid climate with moderate weathering and lower salinity conditions. For both laminated and massive shales from the LCG Fm., the warm and humid climate is beneficial to organic matter (OM) accumulation. Paleoproductivity presents an increasingly positive impact on source rocks when the rock fabric transforms from massive to thick laminae. Overall, lower salinity, humid climate, and strong terrigenous clastic input jointly enhance organic matter (OM) accumulation in both laminated and massive shales. Arid and semiarid climates are beneficial to improving the fractability of both laminated and massive shales. The laminated shale presents a relatively wider average nanopore diameter and lower pore volume than massive samples. These findings provide an important insight into the correlation between organic enrichment, laminae, pore structure, and depositional environment. This study has profound implications for understanding the formation mechanisms of laminated and massive shales in the lacustrine paleoenvironment.

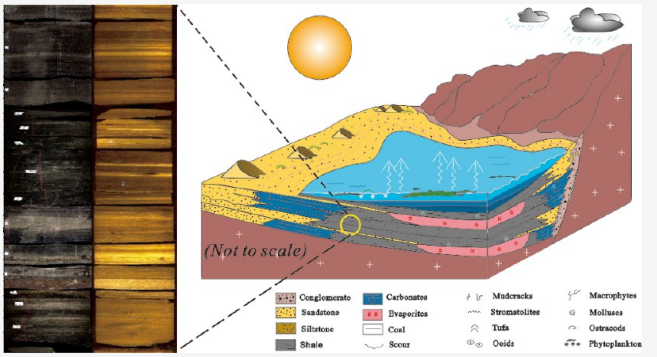

KEYWORDS: *Lucaogou formation, rock fabrics, fractability, organic enrichment, pore structure*

1. INTRODUCTION

Shale contributes to more than 70% of the total sedimentary rocks in the world.[1,2] Lamination (stratification < 10 mm) is the prevailing sedimentary structure of shale deposited by repetitive terrigenous, biological, or chemical components lacking disturbance.[2] The laminae fabric in shale occurs in many forms and is marked by distinct boundaries caused by abrupt alterations in grain size. Although the massive shale is nonlaminated, the massive fabric might correlate with strong bioturbation or dense mudflows alongside the bottom.[3] In recent years, benefiting from a breakthrough in horizontal drilling and hydraulic fracture techniques,[4] oil production from fine-grained sediment reservoirs has become notable. Among the fine-grained rocks, the mineral compositions in laminated and massive shales might be similar; however, their physical properties are different.[5] In addition, the orderly arrangement of mineral and organic matter (OM) makes the pore structure of laminated and massive shales vary at the multiscale.[5,6] Combined with fine scattered silt grains, the laminated,

Received: August 10, 2022
Revised: September 19, 2022
Accepted: September 26, 2022
Published: October 10, 2022

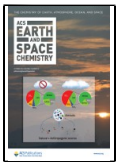

https://doi.org/10.1021/acsearthspacechem.2c00245
ACS Earth Space Chem. 2022, 6, 2530−2551

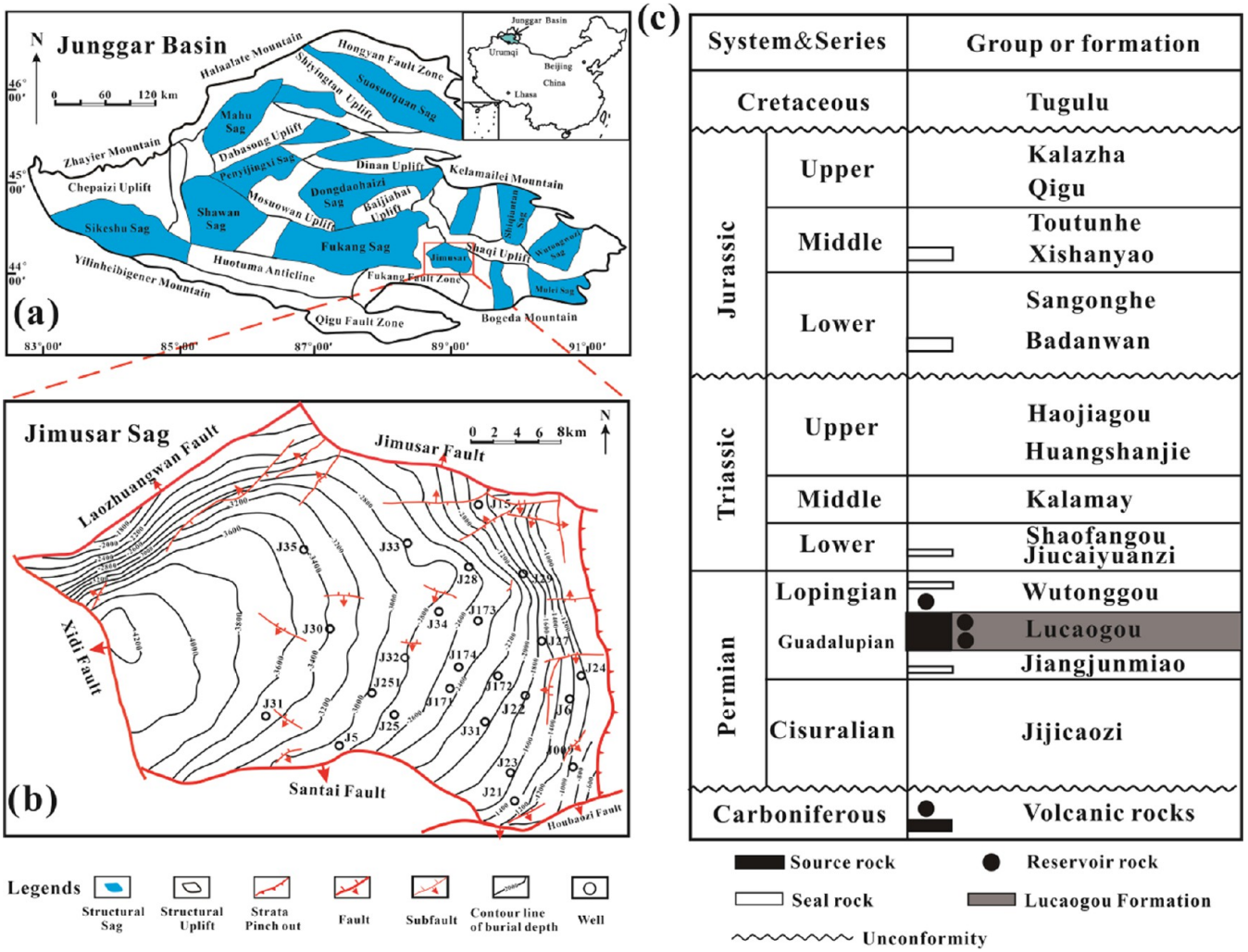

Figure 1. (a) Location of the Junggar Basin during the Middle Permian (modified from Cao et al.[39]). (b) The location of the Jimusar Sag in the southern Junggar Basin (modified from Cao et al.[39]). (c) The generalized stratigraphy of the Jimusar Sag.

organic-rich shale is considered the ideal source rock for shale oil.[5] The research on laminated and massive shales has become a hot topic and is important for accurately evaluating petroleum energy resources.[7−10]

The depositional environment plays an important role in the spatiotemporal variation of shale, including mineral components, hydrocarbon (HC) quality, quantity, rock fabric, and extraction efficiency.[4,11] Mills et al. reported that clay minerals could modulate carbonate diagenesis in the early stage.[12] Cao et al. reported that montmorillonite presents a stronger adsorption capacity than illite and kaolinite.[13] Rahman et al. claimed that the clay and organic matter in the source rock are physically associated.[14] According to M.D. Lewan, claystone and oil shale with laminated and massive rock fabrics are observed in arid and humid climates, respectively.[15] Slatt and Brien et al. observed that OM floccules in fine-grained rocks hydraulically correspond to coarser grains. The pores among floccules are connected, allowing HC transport.[16] However, pelitic rocks might act as potential flow barriers because of their poor fluid conductivity.[17] Xin et al. compared laminated and massive shale samples in the Kongdian Formation (Fm.) and concluded that laminated shale presents better physical properties than massive samples.[5] These studies show that the petroleum accumulation difference caused by paleoenvironment discrepancy should be emphasized.

The term "mixed sediment" is normally related to mixtures of carbonates and siliciclastics in the shallow marine environment.[18] However, the lacustrine mixed sediment is mainly composed of siliciclastic sediments from rivers, carbonate sediments formed in situ in paleolakes, and volcaniclastics transported by wind. The lacustrine mixed sediment is broadly distributed in China across a wide geological age.[19−24] Lacustrine mixed reservoirs have become a new hotspot exploration target for unconventional resources.[22,25] As a huge tectonic lake, the Junggar Basin deposited one of the richest source rocks in the world as the Middle Permian Lucaogou Formation (LCG Fm.).[26] The LCG Fm. is typical for research on the organic matter (OM) input, preservation, and/or dilution in the Permian Junggar Basin.[27] Apart from the OM enrichment, the mixed depositional reservoirs have complex pore structures and rock textures because of strong heterogeneity and multisource minerals.[18,28] Specifically, the three mixed sources are terrigenous clastic grains, tuffaceous materials, and carbonate components.[29] According to Huang et al., the OM burial rate of the LCG Fm. in the Jimusar Sag is 11.2 gC/m^2/yr, and the calculated total organic carbon (TOC) burial during the Middle Permian could have reached 4×10^{12} gC/yr.[30] Although the paleoenvironment of the LCG Fm. in the Jimusar Sag is widely studied from varied perspectives,[29−32] the relationship between

https://doi.org/10.1021/acsearthspacechem.2c00245
ACS Earth Space Chem. 2022, 6, 2530−2551

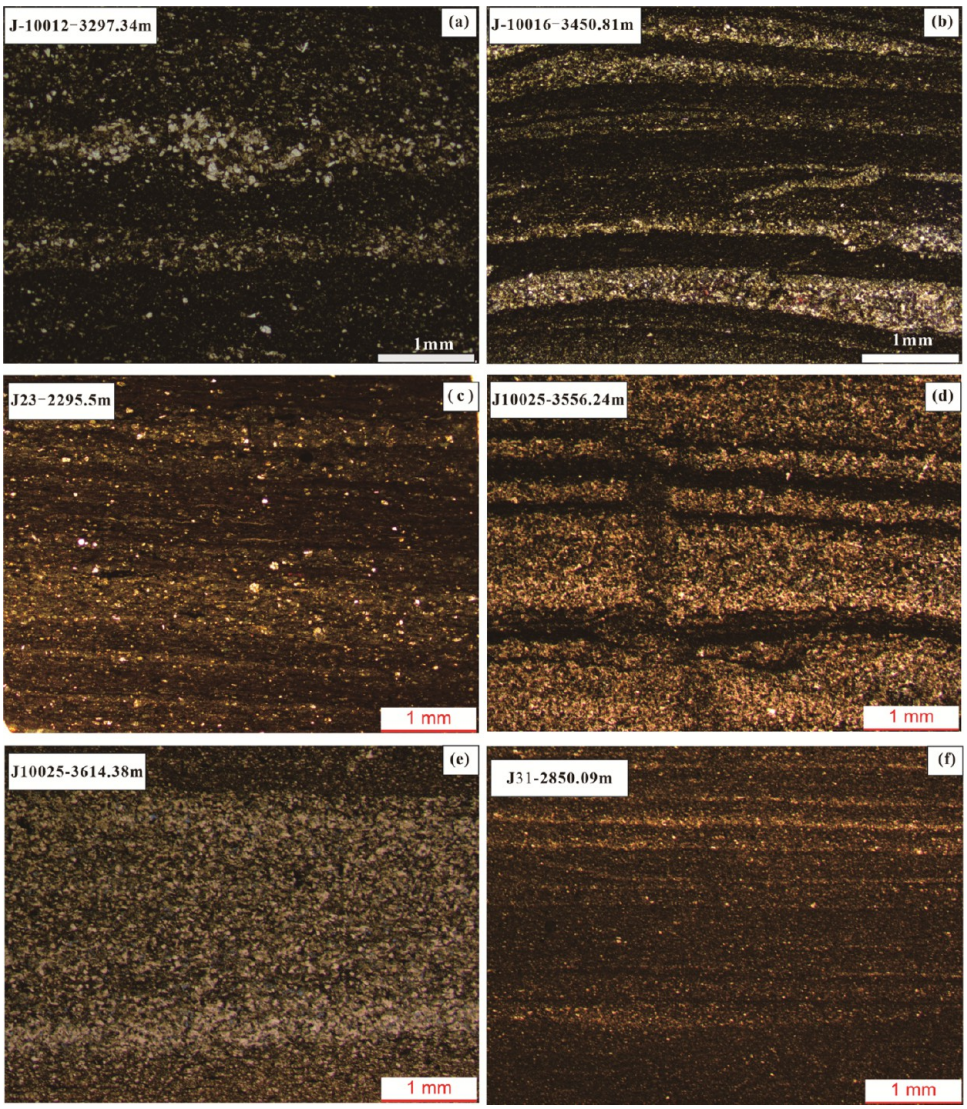

Figure 2. Shale samples with fine and thick laminae under a thin section.

organic enrichment, rock fabric, and deposition conditions of the lacustrine mixed source rock is still unclear.

The paleoenvironment is an important fundamental factor in determining source properties.[33] Varied methods and parameters have been used to clarify the organic enrichment and depositional conditions. The organic enrichment indicators include mineral components, total organic carbon (TOC), and biomarkers.[4,33] The original OM development in the source rock is affected by four major processes: paleoproductivity, paleoredox, clay mineral content, and clastic influx.[4] Some elements are sensitive to the oxygenation level and dynamic balance between organic matter production and decomposition. For example, a high C/N ratio and C_{org}/P values might indicate a high productivity environment. The metallic elements Cu, Zn, and Ni are sensitive to paleoproductivity,[34] and the range of these ratios can reflect the organic source, such as biogenic quartz. Organic preservation indicators including Ni/Co and V/(V + Ni) are extensively used to evaluate paleoredox settings.[4] The mineral elements Al, Zr, and Ti can reflect the terrestrial detrital influx degree and corresponding mineral origin.[35] Considering the fact that some proxies on the paleoenvironment are specific,[36] combined organic and inorganic geochemistry research is more widely used in recent years.[32,37]

In this study, we discuss depositional environment differences between laminated and massive shales in the Permian Lucaogou Formation. These differences are significant for determining variations in geochemical proxies such as OM quality, frackability, and predicting the sweet spot in a mixed lacustrine environment. These findings provide a new perspective on the correlation between organic enrichment, rock fabric development, pore structure, and depositional environment.

2. GEOLOGICAL SETTING

The Junggar Basin was at middle-to-high latitudes in Central Asia during Paleozoic−Cenozoic and experienced continuing tectonic evolution (Figure 1a).[38] The Jimusar Sag is classified as a subordinate structural unit in the southeastern Junggar Basin (Figure 1b).[39] The total area of this sag is approximately 1280 km^2.[2,30]

The Jimusar Sag is a remarkable shale oil source area and has been studied extensively in previous literature studies.[31,39] Tectonically, strata from the Carboniferous to the Quaternary in the Jimusar Sag were deposited, and the sag has experienced Hercynian, Indosinian, Yanshan, and Himalayan orogenies.[30,40] The LCG Fm. in the Jimusar Sag was deposited from 267 to 270

https://doi.org/10.1021/acsearthspacechem.2c00245
ACS Earth Space Chem. 2022, 6, 2530−2551

Table 1. TOC and Rock-Eval Pyrolysis for Lucaogou Source Rocks from the Jimusar Sag, Junggar Basin

sample ID	depth (m)	member	rock fabric	R_o (%)	TOC (%)	S_1(mg/g)	S_2(mg/g)	$S_1 + S_2$ (mg/g)	T_{max} (°C)	HI (mg HC/g TOC)
1-FL	1691.4	$p_2l_1^{2-2}$	laminated	0.87	1.06	1.01	5.77	6.78	435	545.37
2-FL	2541.4	$p_2l_2^{2-1}$	laminated	0.82	5.27	3.22	31.26	34.48	446	592.83
3-FL	2553.1	$p_2l_2^{2-2}$	laminated		11.26	0.74	6.77	7.51	435	60.12
4-FL	2950.5	$p_2l_1^{2-3}$	laminated	0.58	5.99	2.61	37.18	39.79	443	620.39
5-FL	3405.9	$p_2l_2^{2-0}$	laminated	0.72	4.57	4.49	25.51	30.00	438	558.21
6-FL	3577.4	$p_2l_2^{2-2}$	laminated	0.66	10.58	2.32	54.15	56.47	437	511.81
7-TL	2295.5	$p_2l_2^{2-1}$	laminated	0.64	6.12	2.82	35.93	38.75	443	587.48
8-TL	2541.5	$p_2l_2^{2-1}$	laminated		14.42	0.96	16.96	17.92	448	117.61
9-TL	2751.9	$p_2l_2^{1}$	laminated	0.68	2.14	2.47	10.75	13.22	439	501.87
10-TL	2859.2	$p_2l_1^{1}$	laminated	0.54	2.61	11.99	16.88	28.87	434	647.24
11-TL	2953.0	$p_2l_2^{2-3}$	laminated	0.65	11.44	3.20	58.61	61.81	439	512.33
12-MS	2069.5	$p_2l_2^{2-1}$	massive		18.49	1.60	36.35	37.95	442	196.59
13-MS	2577.8	$p_2l_2^{2-0}$	massive	0.86	1.66	1.53	6.18	7.71	442	373.41
14-MS	2298.4	$p_2l_2^{2-2}$	massive	0.71	2.50	1.97	14.93	16.90	446	598.16
15-MS	2756.1	$p_2l_2^{2-0}$	massive	0.84	4.57	1.20	21.76	22.96	445	475.94
16-MS	2853.9	$p_2l_2^{2-2}$	massive	0.81	7.58	2.20	40.04	42.24	445	528.02
17-MS	3171.7	$p_2l_1^{2-0}$	massive	0.68	7.78	4.06	32.79	36.85	442	421.36

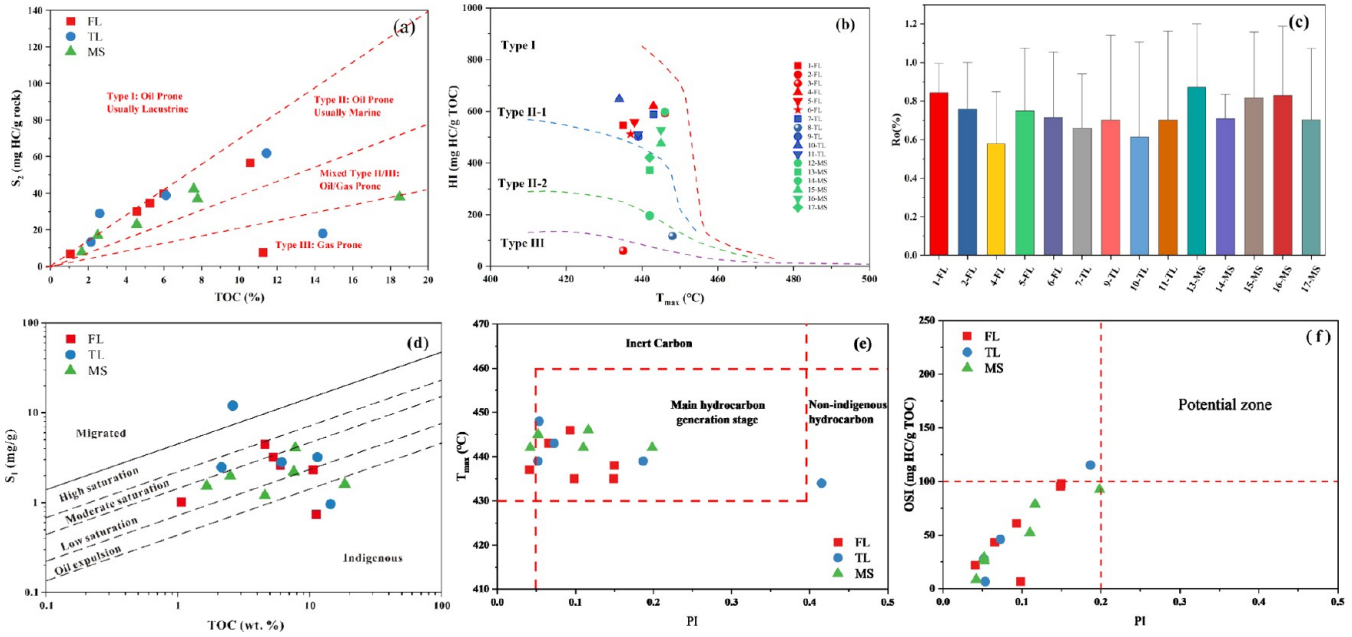

Figure 3. Hydrocarbon generation potential and thermal maturity of Lucaogou source rocks: (a) S_2 versus TOC. (b) T_{max} versus HI (hydrogen index). (c) R_o (vitrinite reflectance). (d) TOC versus S_1. (e) T_{max} versus PI (production index). (f) PI versus oil saturation index (OSI).

Ma and its average sedimentation rate is between 89 and 103 m/Myr.[30] In the balance-filled basin stage, the LCG Fm. was deposited in a restful tectonic setting, and the accommodation fluctuations control the vertical sedimentary thickness change.[41]

During 268 and 270 Ma,[30] the source rocks in LCG Fm. were deposited under saline lacustrine conditions. During this stage, a combination of terrigenous clastic input, volcanic eruption, and multistage hydrothermal activities affected the LCG Fm. In addition, during the Middle Permian, the LCG Fm. experienced fluctuated oxic and anoxic bottom water settings and formed varied laminae combinations (Figure 2).[42] Although the primary productivity is relatively lower than that in modern lakes,[43] the estimated OM burial rate in the LCG Fm. is 11.2 gC/m^2/yr with a huge thickness.[26,30] As a vital carbon pool, the thick organic-rich Lucaogou source rocks in the Jimusar Sag were banked in a deep-to-semideep brackish paleolake. The LCG Fm. consists of both source rocks consisting of black shale (Figure 2) and some uneven quality reservoir rocks including dolomitic siltstone and sandstone.

3. SAMPLES AND METHODS

3.1. Samples. The drilling-core samples are selected from the Middle Permian LCG Fm. (n = 17) from 13 vertical wells drilled in the Jimusar Sag between 1691.4 and 3577.4 m in depth (Figure 1b). The 17 source rock samples include 11 laminated and 5 massive (MS) shale samples. In this study, when the maximum laminae thickness is higher than 1 mm, we define it as thick laminated (TL) shale. In contrast, the shale containing lamina thickness lower than 1 mm is fine-laminated (FL) shale (Figure 2). The massive (MS) shale samples contain no apparent laminae fabric. Based on their laminae thickness,[39] the shale samples are further divided into fine-laminated (FL) samples (n = 6) and thick laminated (TL) samples (n = 5), as listed in Table 1. After being ground-milled homogeneously and

https://doi.org/10.1021/acsearthspacechem.2c00245
ACS Earth Space Chem. 2022, 6, 2530−2551

dried, these powder samples were selected to conduct total organic carbon (TOC) content analysis, Rock-Eval analysis, X-ray diffraction (XRD), nitrogen adsorption (NA) analysis, and element data analysis. For the remaining block samples, organic petrology including vitrinite reflectance measurement (R_o), thin section, and scanning electron microscopy (SEM) was performed on 11 of these samples.

3.2. Methods. A total of 17 samples were used for TOC and Rock-Eval pyrolysis analysis. The operation procedure followed GB/T 19145-2003 and GB/T 18602-2012. The detailed procedure can be found in Li et al.[44] The target parameters for the above tests are T_{max}, S_1, S_2, production index (PI = $S_1/(S_1 + S_2)$), and hydrogen index (HI = S_2/TOC × 100).[45,46] The actual reflectance of 11 samples was tested following ISO 17246:2010. Seventeen selected samples were pretreated and tested for their major, trace, and rare earth elements (REEs). X-ray fluorescence spectroscopy (XRF) was tested to evaluate the major elements. Trace and REEs were analyzed by an Element 6000 inductivity coupled plasma-mass spectrometer (ICP-MS). The mineral components of the 14 dried and crushed samples were analyzed using a Bruker D8 Advance Eco X-Ray diffractometer. The thin-section description method was used to investigate common mineral grains and laminar structure characteristics. The operation procedure followed the China Standard GB/T 5162−1997. In total, 14 samples were selected to conduct low-pressure N_2 adsorption using a Micrometrics ASAP 2020. The surface area was assessed following the Brunauer−Emmett−Teller (BET) model. The pore size distribution (PSD) and pore volume (PV) of laminated and massive shale samples from the LCG Fm. were obtained following the Barrett−Joyner−Halenda (BJH) model.[47,48,50] No unexpected or unusually high safety hazards were encountered.

4. RESULTS

4.1. Bulk Geochemistry. The Lucaogou source rocks contain a wide scope of TOC content (1.06−18.49%, average = 6.94%), and the heterogeneity among different rock fabrics is weak (Figure 3a and Table 1). According to the nomenclature of Peters, (1986),[51] the $S_1 + S_2$ of Lucaogou source rocks ranges between 6.78 and 61.81 mg/g, with an average of 29.42 mg/g, indicating that the organic matter belongs to a good and excellent source rock (Table 1). According to crossplots of HI versus T_{max} and S_2 versus TOC,[52] the Lucaogou samples mainly contain type I-II1 kerogen (Figure 3a,b). T_{max} is a commonly used indicator of thermal maturity.[45] The T_{max} value ranges from 434 to 448 °C (average 441 °C), showing a narrow thermal maturity range from early mature to the peak oil window. The PI (PI = $S_1/(S_1 + S_2)$) values (0.04−0.42, average 0.11) also reflect the relatively low maturity stage. In addition, the R_o value of the samples (0.54−0.87%, average 0.72%) is consistent with the aforementioned thermal maturity indicators (Figure 3c)[53] and previous studies.[42]

Interestingly, the crossplot of S_1 versus TOC suggests that the Lucaogou Formation source rocks contain limited S_1 values mainly in the areas presenting oil expulsion to low saturation (Figure 3d). Most FL, TL, and MS source rock samples are in the main HC generation stage (Figure 3e). The crossplots of the oil saturation index (OSI = S_1/TOC × 100) versus PI confirm that free oil content in both laminated and massive source rocks is relatively low (Figure 3f). Overall, both source rocks from the Permian Lucaogou Formation have a good-to-excellent HC generation potential, and the samples have entered the main HC

Table 2. XRD Results of Selected Laminated and Massive Shale Samples

sample ID	clay	glauberite	cristobalite	aragonite	quartz	potassium feldspar	plagioclase	pyroxene	calcite	dolomite	ankerite	pyrite	hematite	siderite	anhydrite
1-FL	15.60				13.70		0.90		12.90				56.90		
2-FL	27.80	9.50			34.40		5.50		4.40	15.50		1.60		1.40	
4-FL	11.80				15.60	1.70	16.40		39.10	10.30					5.10
5-FL	27.00	10.90			19.90		12.50		13.30	12.50		2.50		1.60	
6-FL		6.20			16.20		12.30		45.40	18.90				1.00	
7-TL	45.80			7.60	23.60		3.70		19.40						
9-TL	13.60				12.10				16.80	57.50					
10-TL					4.50		26.90		6.20		62.40				
11-TL	8.30			3.30	8.80		10.20		17.00		18.00		30.90		3.40
13-MS	15.30		1.00		5.40		1.30		58.20	17.90		0.90			
14-MS	56.70					4.60	7.90	12.70		18.10					
15-MS	13.40				6.30		1.10		19.10	4.90		55.20			
16-MS	31.10				27.00	6.20	9.40		7.20		17.00			2.10	
17-MS	11.80				11.00		9.80		15.00	36.30		8.70	6.50		0.90

https://doi.org/10.1021/acsearthspacechem.2c00245
ACS Earth Space Chem. 2022, 6, 2530−2551

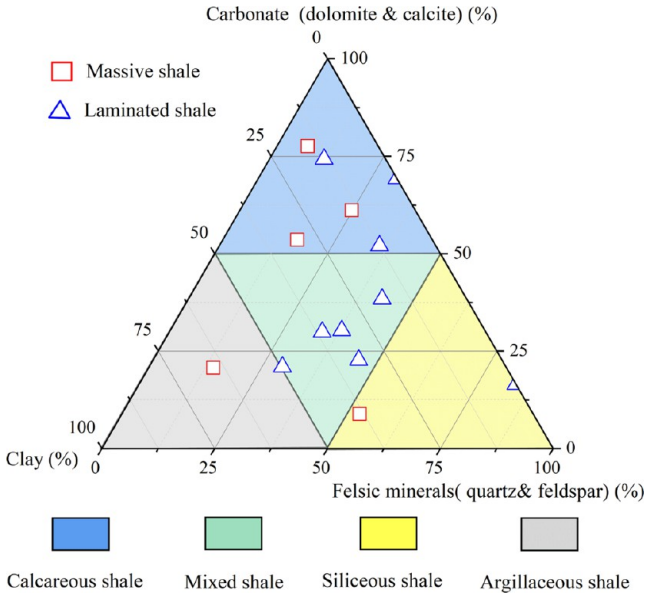

Figure 4. Classification representing source rock lithofacies based on the mineralogical assemblage of selected Lucaogou source rock samples.

generation stage. However, the free oil content (e.g., S_1 and OSI) is relatively low in the source rocks.

4.2. Lithology and Mineralogy. According to the results from whole rock XRD analysis, the calcite content in these samples is found from 4.40 to 58.20%, with an average value of 21.08%. The dolomite content is between 4.90 and 57.50%, with an average value of 21.32%. The clay mineral is between 8.30 and 56.70%, with an average value of 23.18%. For the fine-laminated shale samples, the average contents of calcite and dolomite are similar to those for massive samples. The content of anhydrite is least in massive shale samples, and the massive source rock has higher pyrite content than fine and thick laminated shale (Table 2). According to the ternary graph based on carbonate, clay, and felsic mineral contents,[5] the laminated shale mainly belongs to mixed shale and calcareous shale, and the massive samples are mainly scattered in the calcareous shale, argillaceous shale, and siliceous shale (Figure 4).

4.3. SEM Morphological Characteristics. SEM images of source rock samples show OM, mineral components, and the related pore networks. In our study, the SEM was engaged to distinguish the pore morphology of the source rock matrix, and the typical pore images are shown in Figure 5.

Based on the images, we found four typical pore types that existed in Lucaogou source rock samples (Figure 5), including residual interparticle pores (RIPs), dissolution pores (DPs), clay-dominated pores (CDPs), and fracture and pores (FPs). The SEM assessment is consistent with the semiquantitative mineral results derived from XRD (Table 2). Specifically, the results indicate that Lucaogou source rocks are mainly consistent with calcite, dolomite, feldspar, and clays (kaolinite, illite, and chlorite; Figure 5a,c,d). Organic matter pores are not widely observed, and some organic matter pores are seen as sponge-like with varied pore diameters (Figure 5b). The size of RIPs is commonly larger than 10 μm (Figure 5d). DPs are mainly due to the dissolution of particles or matrix by the acid fluid. The pore network of dissolution pores is more complicated, and the connectivity is stronger than that in interparticle pores. The size of dissolution pores is commonly less than 20 μm (Figure 5a). There are also a large number of pores associated with clay minerals, which are defined here as clay-dominated pores (CDPs). Their size is generally less than

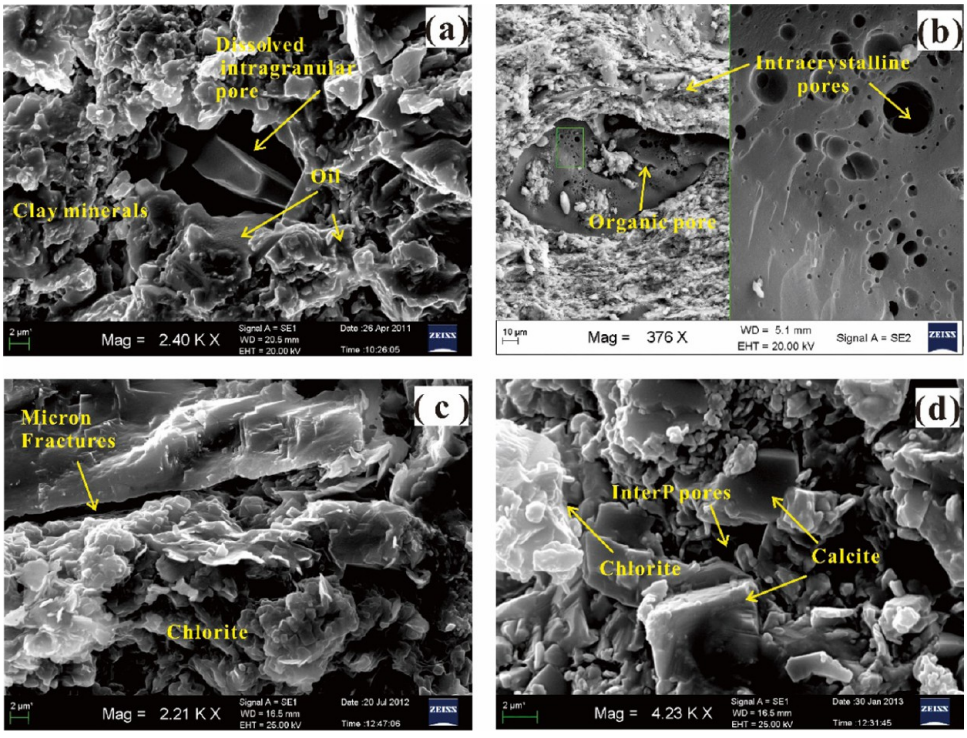

Figure 5. Field emission scanning electron microscopy (FE-SEM) images of different types of pores in the immature−mature source rocks in the Lucaogou Formation: (a) dissolved macropores with an oil coating and associated intercrystalline pores; (b) organic matter with intracrystalline pores, (c) chlorite clay assemblage with microfractures between clay and feldspar; and (d) calcite and chlorite minerals with interparticle pores.

https://doi.org/10.1021/acsearthspacechem.2c00245
ACS Earth Space Chem. 2022, 6, 2530−2551

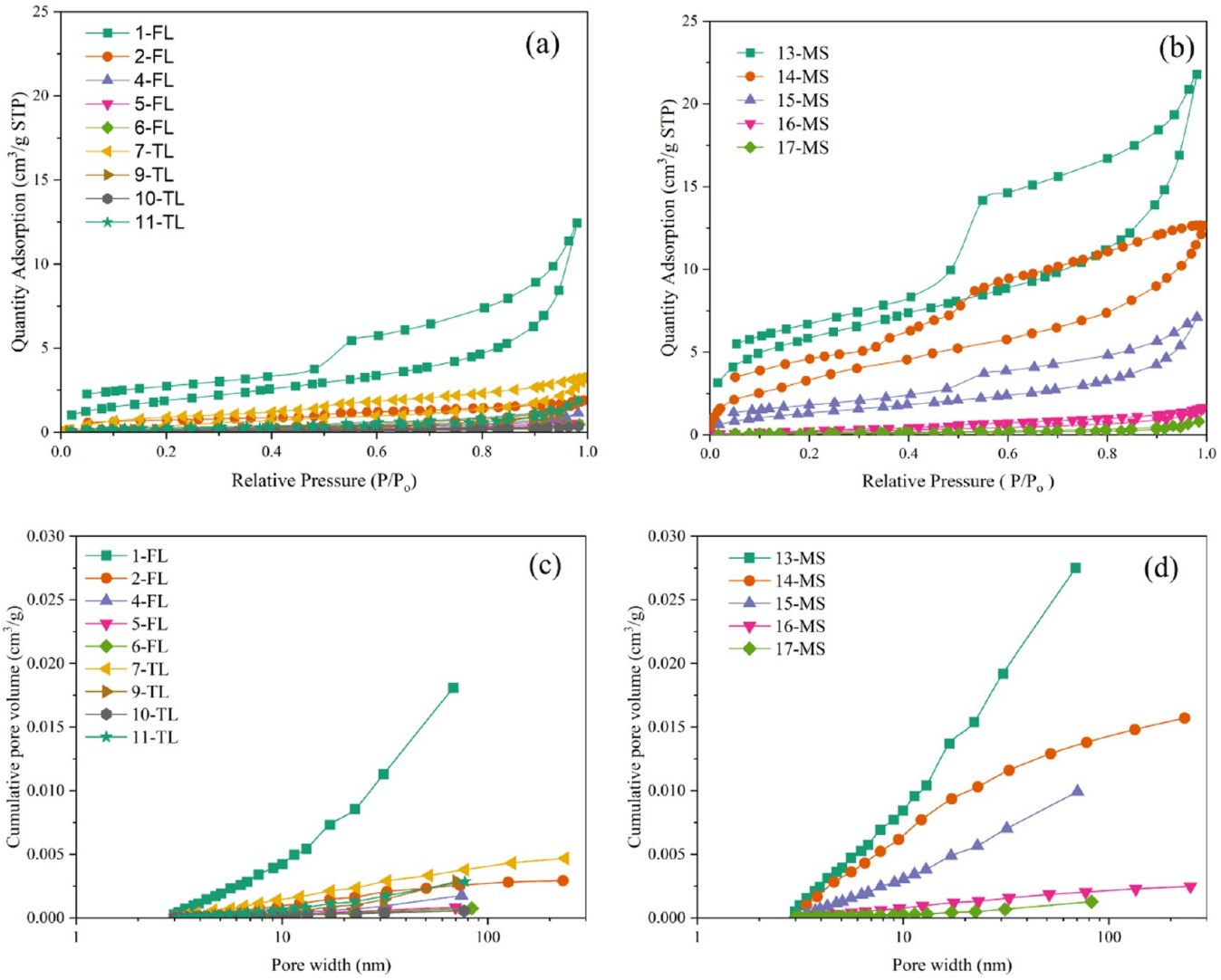

Figure 6. Low-pressure N_2 adsorption/desorption isotherms of (a) FL and TL shales and (b) MS shale. The cumulative pore volume of (c) FL and TL shale and (d) MS shale samples from the Lucaogou Formation.

Table 3. Pore Characterization Parameters Estimated from the Low-Pressure N_2 Adsorption Isotherm Experiment

sample ID	BET-SSA (m^2/g)	total PV (cm^3/g)	mesopore volume (cm^3/g)	macropore volume (cm^3/g)	average pore diameter (nm)
1-FL	7.0120	0.0193	0.0113	0.0068	11.000
2-FL	0.4610	0.0029	0.0023	0.0006	25.530
4-FL	0.4260	0.0018	0.0009	0.0008	16.720
5-FL	0.2250	0.0008	0.0006	0.0002	14.600
6-FL	0.1690	7.2170	0.0005	0.0003	17.080
7-TL	0.9328	0.0050	0.0033	0.0014	21.520
9-TL	0.6725	0.0029	0.0015	0.0014	17.380
10-TL	0.1666	0.0005	0.0004	0.0001	12.850
11-TL	0.7351	0.0029	0.0017	0.0011	15.790
13-MS	21.4900	0.0338	0.0192	0.0083	6.289
14-MS	1.3670	0.0188	0.0129	0.0028	5.493
15-MS	5.0580	0.0110	0.0070	0.0029	8.710
16-MS	0.9302	0.0024	0.0018	0.0006	10.140
17-MS	0.2515	0.0013	0.0007	0.0006	20.020

500 nm (Figure 5c). The FPs are mainly due to the fracture of the brittle material, nanoscaled in width and micron-scaled in length (Figure 5c).

4.4. Low-Pressure N_2 Adsorption. Low-pressure N_2 adsorption was applied to analyze the structural character and storage space of the pores.[49] The N_2 adsorption isotherms of laminated and massive shales are revealed in Figure 6. The isotherm curves mainly belong to type IV according to the classification from the International Union of Pure and Applied Chemistry (IUPAC).[49] The hysteresis loop of source rock

https://doi.org/10.1021/acsearthspacechem.2c00245
ACS Earth Space Chem. 2022, 6, 2530−2551

Table 4. Major Element Concentrations in Laminated and Massive Shales from LCG Fm.[a]

sample ID	depth (m)	member	rock fabric	SiO_2 (%)	Al_2O_3 (%)	MgO (%)	Na_2O (%)	K_2O (%)	P_2O_5 (%)	TiO_2 (%)	CaO (%)	Fe_2O_3 (%)	MnO (%)	LOI (%)
1-FL	1691.4	$p_2l_1^2$	laminated	60.87	8.08	2.81	0.66	0.88	0.06	0.28	16.84	1.75	0.15	7.63
2-FL	2541.4	$p_2l_2^{2-1}$	laminated	62.63	10.99	4.52	1.33	2.81	0.09	0.53	3.98	3.67	0.11	9.27
3-FL	2553.1	$p_2l_2^2$	laminated	63.75	12.74	2.48	1.64	4.24	0.13	0.63	2.27	4.56	0.06	6.80
4-FL	2950.5	$p_2l_1^{2,3}$	laminated	35.21	7.03	4.48	3.40	1.18	0.13	0.37	20.31	3.30	0.14	24.34
5-FL	3405.86	$p_2l_2^{2-0}$	laminated	62.45	12.22	1.91	2.47	2.84	0.14	0.75	4.26	4.10	0.05	8.77
6-FL	3577.4	$p_2l_2^2$	laminated	54.70	11.01	2.88	3.50	3.20	0.14	0.58	5.63	1.81	0.08	16.60
7-TL	2295.5	$p_2l_2^{2-1}$	laminated	63.87	11.87	2.08	1.02	2.16	0.25	0.60	7.30	4.30	0.11	6.56
8-TL	2541.5	$p_2l_2^{2-1}$	laminated	46.92	9.28	8.21	1.44	1.94	0.09	0.42	11.41	4.70	0.16	15.51
9-TL	2751.93	$p_2l_2^1$	laminated	25.47	5.04	10.55	0.54	0.42	0.08	0.12	23.03	3.66	0.47	30.59
10-TL	2859.2	$p_2l_1^1$	laminated	47.85	10.16	4.17	7.52	0.80	0.07	0.24	8.81	1.40	0.17	18.82
11-TL	2953	$p_2l_2^{2,3}$	laminated	35.54	7.13	6.68	3.33	1.04	0.14	0.36	16.80	2.83	0.11	26.01
12-MS	2069.5	$p_2l_2^{2-1}$	massive	70.01	11.62	1.56	1.12	2.35	0.30	0.62	2.20	3.80	0.04	6.17
13-MS	2577.8	$p_2l_2^{2-0}$	massive	64.09	13.54	3.17	1.12	2.19	0.10	0.69	4.95	4.69	0.05	5.22
14-MS	2298.4	$p_2l_2^2$	massive	69.17	12.76	3.60	1.68	3.49	0.11	0.67	1.18	4.05	0.04	3.38
15-MS	2756.1	$p_2l_2^{2-0}$	massive	68.31	14.97	2.13	0.89	2.91	0.17	0.71	1.35	2.60	0.03	5.83
16-MS	2853.9	$p_2l_2^2$	massive	65.47	10.85	4.40	2.00	3.90	0.13	0.54	0.54	6.40	0.02	4.61
17-MS	3171.7	$p_2l_1^{2-0}$	massive	39.82	8.29	6.82	4.49	1.51	0.11	0.46	10.92	5.32	0.11	21.41

[a]Note: LOI denotes loss on ignition.

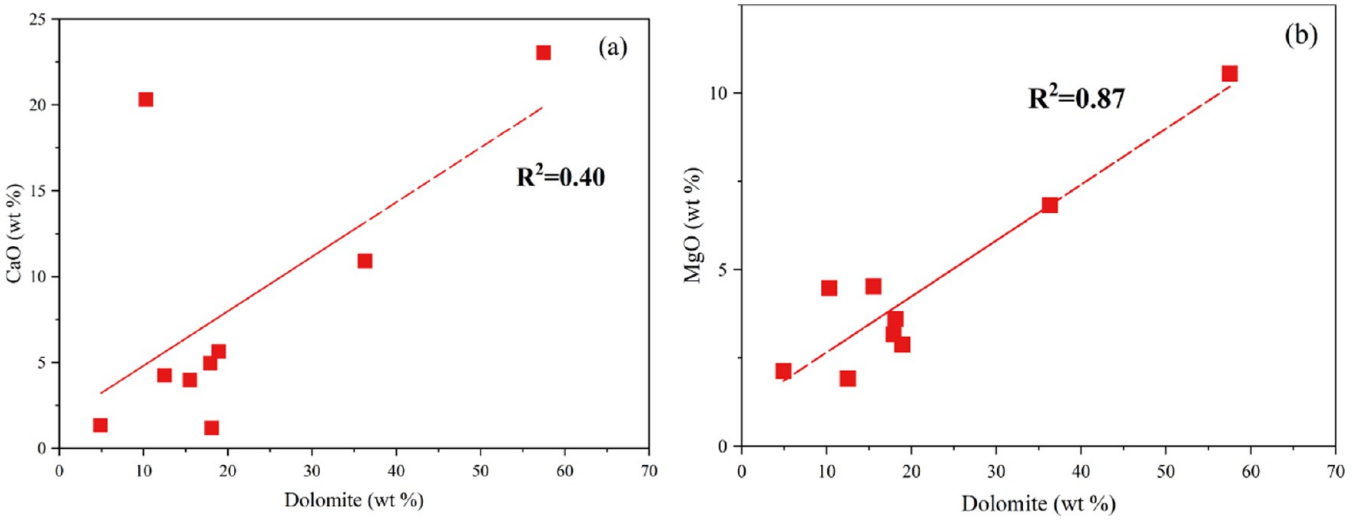

Figure 7. Crossplots of (a) dolomite versus CaO content and (b) dolomite versus MgO content.

samples from the LCG Fm. is mainly categorized by a mix of types H2 and H3,[50] demonstrating that the pore morphology is mainly ink-bottle and slit shapes (Figure 6a,b). The SEM images suggest that the ink-bottle pore morphology is mainly correlated with the dissolution pores and some organic matter pores (Figure 5a,b). Contrary to previous studies,[54] the TOC content in this study presents a negative relationship with the maximum adsorption amount (Table 3), indicating that the organic pores are scarce. The slit-like pores are primarily correlated to the flaky clay minerals such as illite and the pore generated near the boundary of irregular organic matter (Figure 5b). Most shale samples produced closed adsorption loops and present a lower adsorbed volume, suggesting that the pore networks in shales are open (Figure 6a). Moreover, some massive samples present unclosed adsorption loops, suggesting poor connectivity and higher volume of the pore network in massive shale (Figure 6b).

The statistical pore structure indicators assessed from these isotherms are listed in Table 3. Due to the limitation of N_2 adsorption, only the mesopores and macropores with pore diameters between 2 and 300 nm were detected in this study. We only discuss the pore structure in this range. According to the results, the BET-specific surface area (BET-SSA) value is from 0.17 to 21.49 m^2/g, the total PV value is between 0.0005 and 0.0338 cm^3/g, mesopore volume ranges from 0.0004 to 0.0192 cm^3/g, and the average pore diameter is 5.49−25.53 nm, indicating the presence of both mesopores and macropores (Table 3 and Figure 5c,d). However, the majority of the pore volume is contributed by mesopores (69.64%, Table 3). The cumulative pore volume of massive shale presents a higher increase rate than FL and TL shale samples (Figure 6c,d). This is consistent with the lacustrine laminated and massive shales from the Paleogene Kongdian Formation.[5]

4.5. Elements Analysis. Elemental geochemistry is applicable to reconstruct the depositional and diagenetic history of source rocks. For Lucaogou source rocks, SiO_2 is the major component with an average of 55.06%, followed by Al_2O_3 (5.04−14.97%) and CaO (0.54−23.03%, Table 4). The content of MgO, CaO, and Na_2O is higher than post-Archean shales from Australia (PAAS). The higher content of CaO and MgO is probably associated with the high dolomite mineral components

https://doi.org/10.1021/acsearthspacechem.2c00245
ACS Earth Space Chem. 2022, 6, 2530−2551

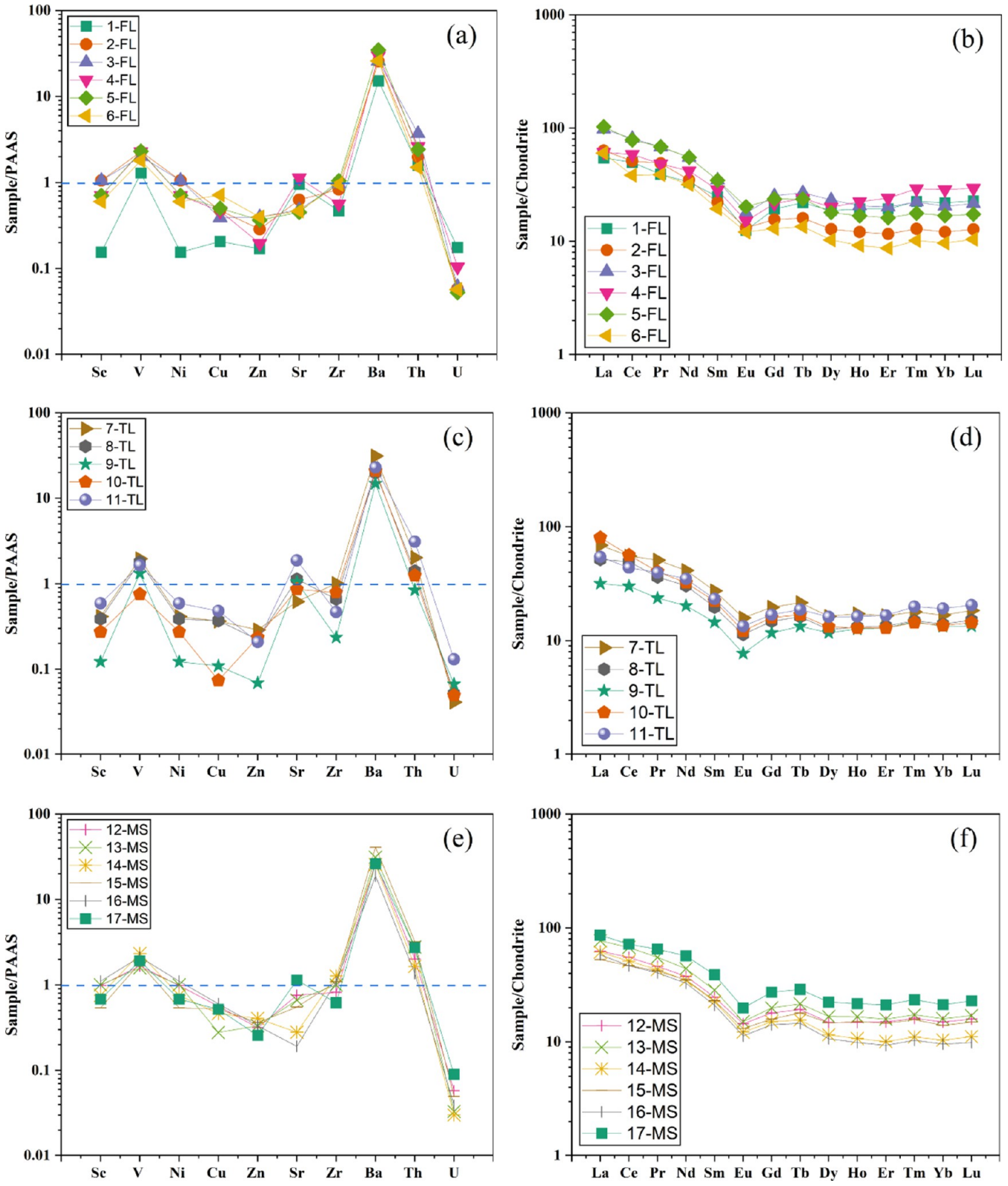

Figure 8. Standardized spider web map. Trace element map of the (a) FL shale, (c) TL shale, and (e) MS shale samples normalized by PAAS (PAAS data from Taylor et al.[55] REE distribution of the (b) FL shale, (d) TL shale, and (f) MS shale standardized by chondrite (chondrite data from Taylor et al.[55]).

in the LCG Fm. This is supported by positive relationships between dolomite and CaO and MgO (Figure 7a,b). This is consistent with the LCG Fm. in the Santanghu Basin.[51] The average content of P_2O_5 and MnO are close to PAAS. The SiO_2, Al_2O_3, TiO_2, Fe_2O_3, and K_2O contents are lower than PAAS.

The chondrite-normalized (CN) REE patterns[55] of laminated and massive shale samples present a downward trend from left to

https://doi.org/10.1021/acsearthspacechem.2c00245
ACS Earth Space Chem. 2022, 6, 2530−2551

Table 5. Trace and REE Element Data for Laminated and Massive Shale Samples from LCG Fm. in the Jimusar Sag

sample ID	La_{CN}/Yb_{CN}	Gd_{CN}/Yb_{CN}	Eu_{CN}/Eu^*_{CN}	Ce_{CN}/Ce^*_{CN}	CIA	C-value	Sr/Cu	Rb/Sr	Sr/Ba	Y/Ho	U_{EF}	Mo_{EF}	C_{org}:P	Th/Sc	Zr/Sc	Fe/Ti	(Fe + Mn)/Ti
1-FL	2.48	0.88	0.57	1.08	78.62	0.09	35.42	0.04	2.80	28.15	6.64	2.04	44.39	0.68	13.61	7.32	7.99
2-FL	5.25	1.29	0.71	0.92	66.82	0.38	10.21	0.19	1.09	26.79	1.62	17.35	146.17	0.67	19.08	8.02	8.29
3-FL	4.79	1.24	0.60	0.99	62.91	0.68	9.53	0.37	0.83	26.88	1.48	2.41	219.35	0.87	15.40	8.48	8.61
4-FL	2.14	0.75	0.61	1.07	46.82	0.12	18.53	0.04	1.70	29.64	4.52	18.71	118.34	0.51	7.45	10.44	10.92
5-FL	6.10	1.40	0.71	0.94	61.15	0.46	6.89	0.32	0.58	27.43	1.31	3.32	81.51	0.84	24.53	6.39	6.48
6-FL	6.24	1.34	0.76	0.79	51.94	0.15	4.96	0.29	0.80	27.15	1.58	29.91	201.35	0.63	27.31	3.62	3.80
7-TL	4.11	1.17	0.68	0.93	73.89	0.41	12.94	0.16	0.88	28.88	1.06	1.95	63.47	0.57	19.38	8.39	8.62
8-TL	3.69	1.06	0.66	1.14	65.79	0.23	23.43	0.07	2.54	27.45	1.70	3.82	392.57	0.30	9.62	13.12	13.62
9-TL	2.38	0.88	0.59	1.10	77.18	0.11	73.12	0.02	3.13	30.50	4.06	5.32	66.88	0.30	5.60	35.28	40.28
10-TL	5.92	1.17	0.65	0.99	39.07	0.07	88.98	0.05	1.84	25.90	1.49	2.40	100.48	0.39	16.82	6.88	7.78
11-TL	2.84	0.88	0.68	0.94	48.05	0.11	29.95	0.03	3.64	28.80	5.61	16.72	217.51	0.75	7.60	9.07	9.46
12-MS	4.19	1.20	0.69	1.03	71.66	0.74	10.28	0.15	1.24	25.53	1.52	3.34	161.30	0.53	14.50	7.10	7.18
13-MS	4.84	1.25	0.63	1.03	75.36	0.51	18.28	0.19	0.95	26.01	0.74	2.24	44.31	0.79	19.22	7.90	7.98
14-MS	5.91	1.45	0.66	0.99	68.04	0.62	4.63	0.61	0.49	26.60	0.72	4.96	60.30	0.43	22.72	7.01	7.08
15-MS	3.78	1.14	0.68	0.99	76.50	0.57	8.07	0.30	0.60	25.07	1.01	2.07	70.95	1.10	25.42	4.25	4.30
16-MS	6.09	1.48	0.66	0.96	64.41	0.93	2.44	0.88	0.45	26.40	1.10	14.14	149.28	0.58	31.15	13.84	13.90
17-MS	4.06	1.29	0.61	0.96	44.15	0.24	16.82	0.06	1.94	30.11	3.32	19.03	174.68	0.63	9.57	13.44	13.74

right (Figure 8b,d,f). The total REE ($\sum$REE) concentrations are between 67.50 and 172.08 ppm. The CN REE patterns of laminated and massive shales suggest that the light rare earth elements (LREEs, La to Eu) experienced fractionation and enrichment supported by high La_{CN}/Yb_{CN} ratios (2.14−6.24) in both laminated and massive shale samples from the LCG Fm. (Table 5). However, the heavy Gd_{CN}/Yb_{CN} values are relatively low (0.75−1.48) for the Lucaogou source rock samples, demonstrating the enrichment of LREEs. A negative Eu anomaly (Eu_{CN}/Eu^*_{CN}) is prominent in both laminated and massive shales with an average value of 0.66, representing a relatively reducing environment setting.[56] No apparent Ce anomaly was observed, and the average Ce_{CN}/Ce^*_{CN} value is 0.99 (Figure 8b,d,f). This is consistent with previous studies.[57]

5. DISCUSSION

5.1. Paleoenvironmental Reconstruction. *5.1.1. Paleoclimate and Palesalinity.* The chemical index of alteration (CIA) is sensitive to remark the chemical weathering degree and paleoclimate.[58−60] According to Nesbitt and Young, when the CIA value is at 50−65, the climate is cold and dry at low chemical weathering. When CIA is at 65−85, The climate is warm and humid under moderate chemical weathering. When the value is 85−100, it represents a hot and humid climate under strong chemical weathering.[59,61] In the Jimusar Sag, the CIA values of all of the Lucaogou source rocks range between 39.07 and 78.62, and the average value is 63.08 (Figure 9a). Specifically, the calculated CIAs of FL shale vary from 46.82 to 78.62, with an average of 46.82. The CIAs of TL shale vary from 39.07 to 77.18, with an average of 60.79, while the MS shale samples vary from 44.15 to 76.50, and the average value is 66.69, which is close to the value of PAAS (CIA = 69.0, referred from Kasanzu et al.).[62]

In addition, the trace elements (Sr, Rb, and Cu) and their ratios (Rb/Sr, Sr/Cu) are widely applied to reconstruct the sedimentary environment at a specific time.[44,63] Specifically, Rb/Sr ratios > 0.5 and < 0.5 represent an arid and humid climate. Furthermore, Sr/Cu ratios > 10 imply a dry and hot climate, whereas Sr/Cu ratios in the range of 1−10 suggest a warm and humid climate.[64] Core test analyses of Lucaogou source rocks from the 11 wells show that Rb/Sr and Sr/Cu ratios are generally at 0.02−0.88 (average 0.22) and 2.44−88.98 (average 22.03), respectively (Table 5). This suggests that the source rocks from the LCG Fm. were deposited in both humid and hot climates. The *C*-value is a practical indicator of paleoclimate. The *C*-value is expressed as eq 1

$$C - \text{value} = \Sigma(\text{Fe} + \text{Mn} + \text{Cr} + \text{Ni} + \text{V} + \text{Co}) / \Sigma(\text{Ca} + \text{Mg} + \text{Sr} + \text{Ba} + \text{K} + \text{Na}) \quad (1)$$

C-values < 0.2, 0.2−0.4, 0.4−0.6, 0.6−0.8, and > 0.8 indicate arid, semiarid, semiarid to semihumid, semihumid, and humid climates, respectively.[65]

For Lucaogou source rocks, the majority of FL and TL shale samples were plotted in the arid and semiarid region (Figure 9b), while the MS shale samples were mainly in the semihumid and humid region (Figure 9b). Overall, the climate indices used in this study indicate that the Lucaogou TL shale samples are commonly deposited in the hot and dry climate with weak weathering; however, the MS shale is more commonly formed in a relatively warm and humid climate under moderate chemical weathering.

https://doi.org/10.1021/acsearthspacechem.2c00245
ACS Earth Space Chem. 2022, 6, 2530−2551

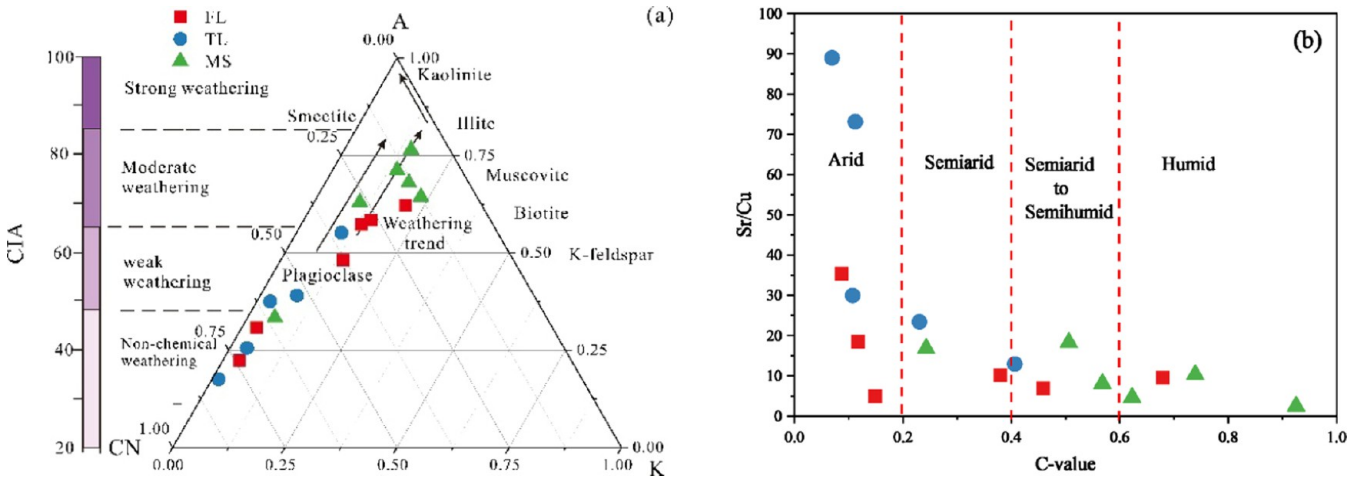

Figure 9. (a) CIA versus A-CN-K ternary diagram. (b) *C*-value versus Sr/Cu.

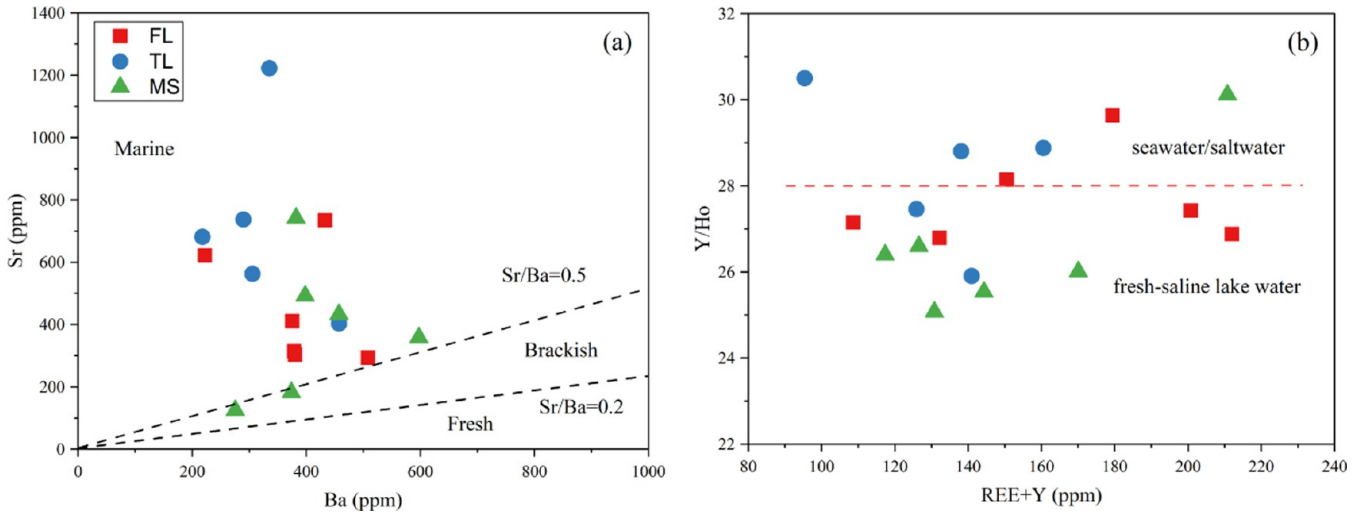

Figure 10. Correlation between (a) Ba versus Sr content and (b) REE + Y versus Y/Ho of the Lucaogou source rocks.

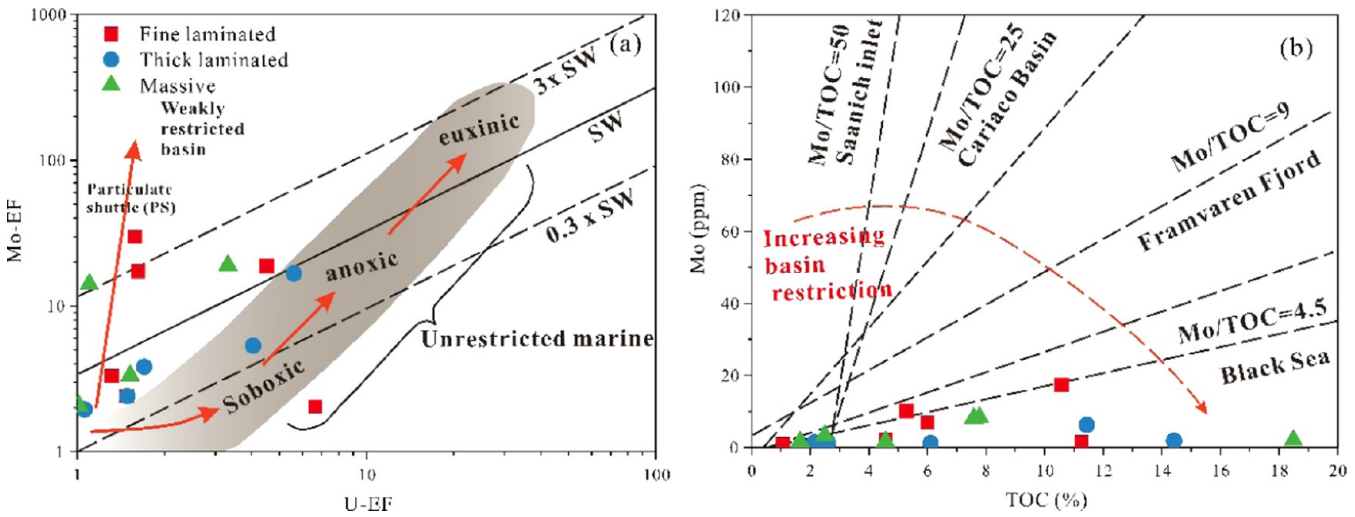

Figure 11. (a) U_{EF} versus Mo_{EF}.[7373] (b) TOC versus Mo content.

The Sr/Ba ratio is deemed to be a practical indicator of paleosalinity.[66] The value increases with rising salinity. Generally, for the lacustrine environment lacking seawater intrusion, a small Sr/Ba ratio signifies freshwater, Sr/Ba values at 0.5−1.0 imply brackish water, and Sr/Ba values > 1.0 imply brackish water in an arid climate.[67,68] The Sr/Ba values of the Lucaogou source rock samples show a broad range from 0.45 to 3.64, with an average of 1.50, suggesting a paleoenvironment

https://doi.org/10.1021/acsearthspacechem.2c00245
ACS Earth Space Chem. 2022, 6, 2530−2551

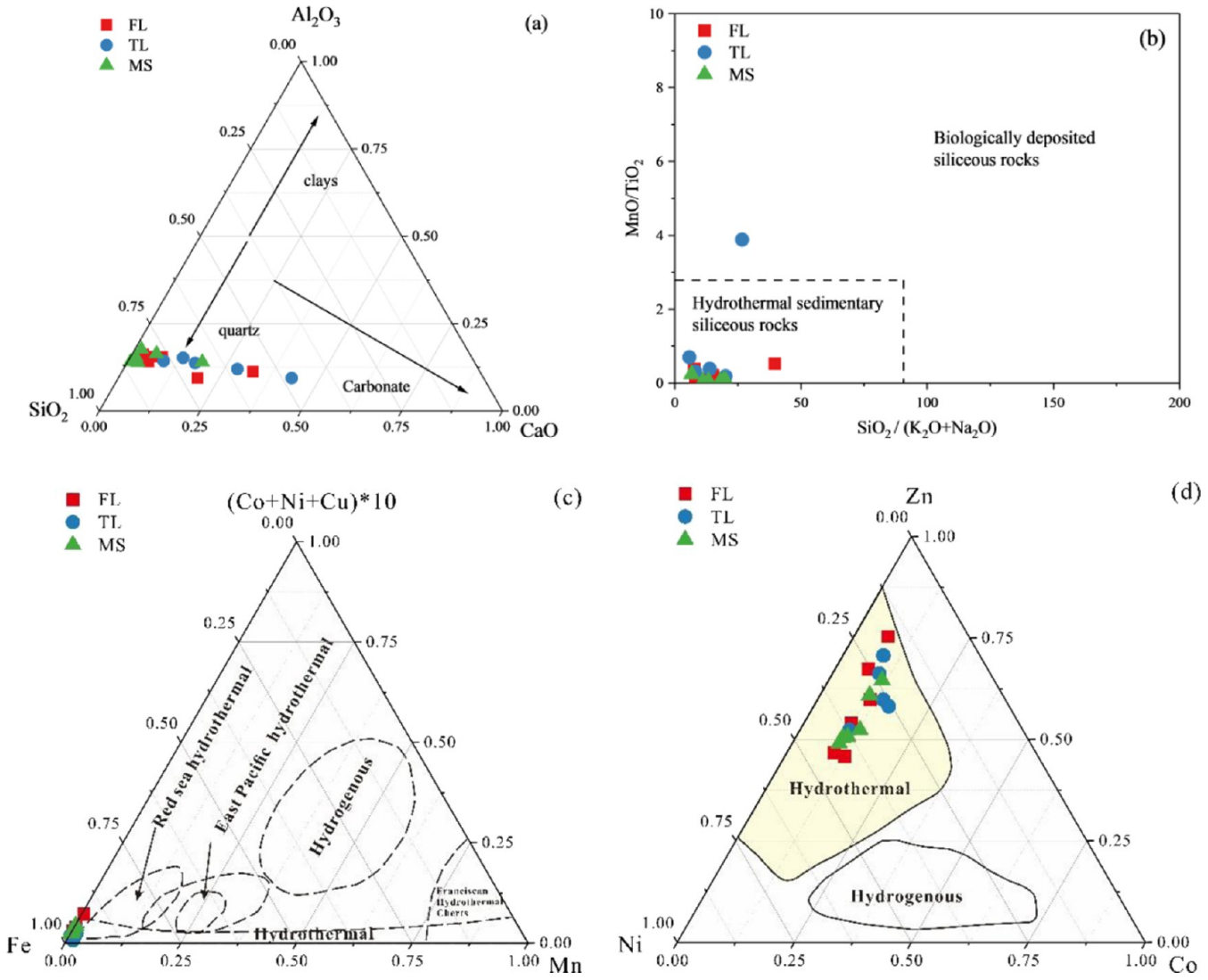

Figure 12. (a) $SiO_2-Al_2O_3-CaO$, (b) $SiO_2/(K_2O+Na_2O)$ versus MnO/TiO_2, (c) ternary diagram Fe−Mn−(Co+Ni+Cu) × 10, and (d) ternary diagram of Zn−Co−Ni.

with inconstant salinity. The average Sr/Ba ratios for TL shale, FL shale, and MS shale are 2.41,1.30, and 0.94 respectively (Figure 10a and Table 5). This indicates that the MS shale is preferred to form in lower salinity conditions than FL and TL shales (Figure 10a). Y/Ho > 28 can signify lake water salinity that is analogous to seawater.[69,70] The average Y/Ho ratios for source rocks with TL, FL, and MS are 28.31, 27.67, and 26.62, respectively (Figure 10b). Overall, the paleolake salinity shows a positive correlation with laminae thickness.

5.1.2. Paleoredox Conditions. The redox surroundings play a crucial role in the formation and conservation of OM in oil shale.[71] For the lacustrine environment, high-frequency variations in the climate might influence lake dynamics and make the redox conditions more complicated. Although there are no unanimous element thresholds in all sedimentary systems, we combine the trace element enrichment factors (EF) and the organic carbon-to-total phosphorus (C_{org}:P) ratio to elucidate the benthic redox conditions.[36,68] The trace element enrichment factors (EFs) are computed as eq 2 following the previous literature[72]

$$X_{EF} = [(X/Al)_{sample}/(X/Al)_{PAAS}] \quad (2)$$

where X_{sample} and X_{PAAS} are the contents of element X of the selected sample and PAAS, respectively.[55] According to previous studies,[72,73] Mo_{EF} and U_{EF} < 10 suggest suboxic conditions, while higher values signal euxinic water bodies. The Lucaogou source rock samples have Mo_{EF} values of 1.95−29.91 (average = 8.81) and U_{EF} ranging from 0.72 to 6.64 (average = 2.32) (Table 5). These values suggest that the LCG laminated and massive shales were primarily deposited in suboxic conditions (Figure 11a). Furthermore, the TOC-Mo crossplot shows that the Lucaogou laminated and massive shales have low Mo/TOC ratios, which was caused by high TOC content and low Mo concentration, indicating a restricted deposition environment (Figure 11b). Overall, the LCG Fm. in the Jimusar Sag was deposited in oxic and anoxic water bodies, and the oxygen content is higher than that in other alkaline lakes such as the Fengcheng Fm in the Santanghu Basin.[42]

The C_{org}/P ratio is a redox indicator defined by Algeo and Ingall

$$C_{org}/P = (TOC/12)/(P/30.97) \quad (3)$$

The higher C_{org}/P ratio usually indicates anoxic conditions.[74] Generally, C_{org}/P > 100 represents the reducing conditions,

https://doi.org/10.1021/acsearthspacechem.2c00245
ACS Earth Space Chem. 2022, 6, 2530−2551

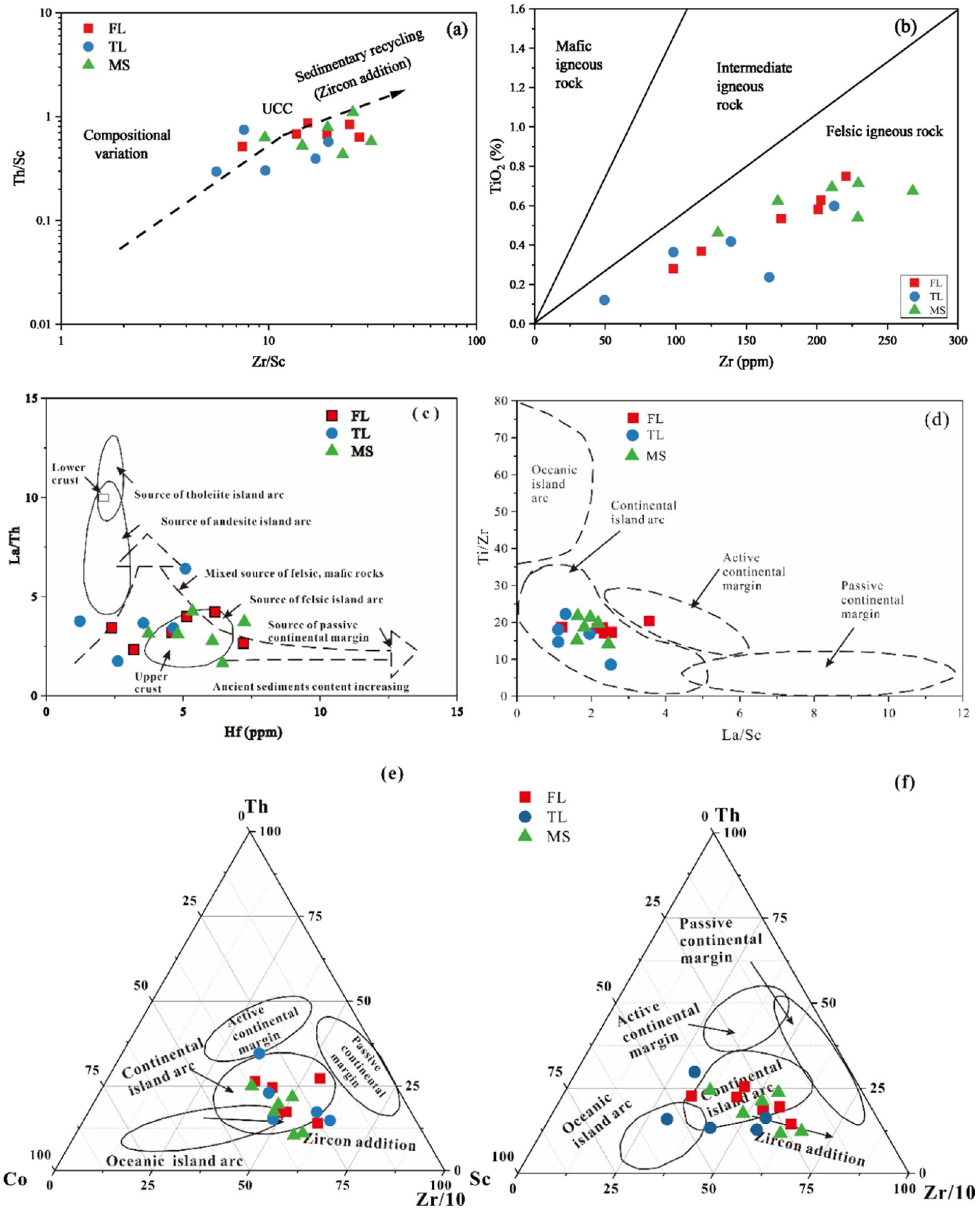

Figure 13. Compositional variation in the sample sets in Lucaogou Formation samples suggests the involvement of the recycled material. (a) Zr/Sc versus Th/Sc plot,[61] (b) Zr versus TiO_2,[78] (c) Hf versus La/Th,[79] and (d) La/Sc versus Ti/Zr plots.[81] Ternary plots of (e) Co−Th−Zr/10 and (f) Sc−Th−Zr/10.[81]

whereas $C_{org}/P < 50$ is typical of oxygenated conditions.[36] In this study, C_{org}/P ratios of Lucaogou source rocks range from 44.31 to 392.57 (average = 136.05). The average values of source rocks with TL, FL, and MS rock fabrics are 168.18, 135.18, and 110.14,

https://doi.org/10.1021/acsearthspacechem.2c00245
ACS Earth Space Chem. 2022, 6, 2530−2551

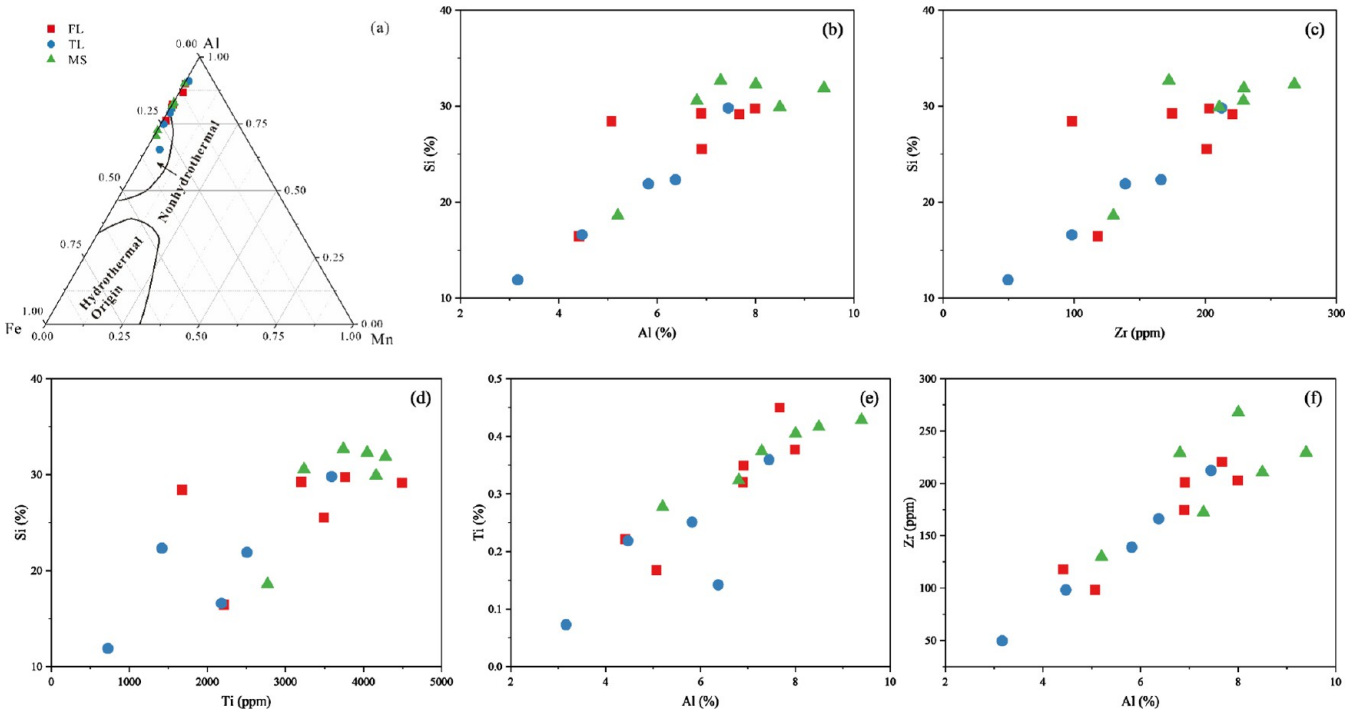

Figure 14. Relationship between terrigenous debris inputs indicating elements and Si to show the silica origin of Lucaogou source rocks. (a) Al−Fe−Mn ternary diagram; (b) Al versus Si; (c) Zr versus Si; (d) Ti versus Si; (e) Al versus Ti; (f) Al versus Zr.

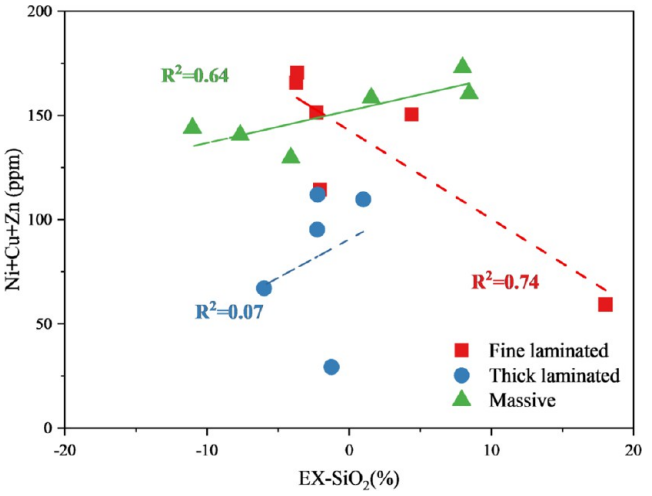

Figure 15. Crossplot between EX-SiO_2 and Ni+Cu+Zn contents of shale and mudstone.

respectively (Table 5). The relatively high C_{org}/P ratio in laminated shale than that in massive shale is explained by the following three reasons: (1) the weak bacteria activity in anoxic conditions restricted the storage of P in laminated shale, (2) extensive P regeneration from sedimentary organic matter in massive shale, and (3) the presence of laminae enhanced preservation capacity than the bioturbated massive fabric.[75] These data are consistent with the aforementioned redox proxies (Figure 11) and previous conclusions in the literature.[42,76]

5.1.3. Hydrothermal Alteration. The crossplot of $SiO_2/(K_2O + Na_2O)$ versus MnO/TiO_2 is applied to discriminate hydrothermal origin from the biological origin of siliceous rocks.[77] Considering that the Lucaogou source rock samples are large in siliceous components (Figure 12a), the above crossplot is applicable in this study. The majority of data in this study are plotted in the hydrothermal zone of the $SiO_2/(K_2O + Na_2O)$ versus MnO/TiO_2 crossplot (Figure 12b). Moreover, the ternary graph of Mn versus Fe versus (Cu + Co + Ni) × 10 of the same samples was also plotted in the hydrothermal zone and is predominantly similar to the Red Sea hydrothermal model (Figure 12c). The evidence of hydrothermal activities is also from the ternary diagram of Ni−Co−Zn (Figure 12d). The above parameters indicate that the source rocks from the LCG Fm. in the Jimusar sag experienced weak hydrothermal activities. This is supported by previous studies.[76]

5.2. Provenance and Tectonic Origin. *5.2.1. Tectonic Origin of Lucaogou Source Rocks.* The Al_2O_3/TiO_2 value of the majority of clastic sediments is effectively used to speculate their source rock composition. The ratios at 3−8, 8−21, and 21−70 represent the mafic origin, the intermediate origin, and the felsic igneous origin, respectively.[78] McLennan et al. used the Th/Sc−Zr/Sc crossplot to discriminate the heavy mineral content, compositional maturity, and sediment sorting degree.[61] Moreover, the TiO_2/Zr values and La/Th−Hf values[79] are also valid to elucidate source rock types.[80]

The Al_2O_3/TiO_2 values of the source rocks span between 16.30 and 42.91 (average 22.72), representing the intermediate and felsic igneous origins. The Th/Sc and Zr/Sc ratios of the Lucaogou source rock samples vary at 0.30−1.10 (average 0.62) and 5.60−31.15 (average 17.00), respectively (Table 5). This suggests strong sedimentary recycling and clear zircon addition (Figure 13a). In addition, the crossplot of TiO_2 versus Zr[78] implies a felsic igneous origin for the Permian Lucaogou Formation (Figure 13b). The La/Th−Hf crossplot (Figure 13c) signifies that the source rocks mainly originated from mixed felsic and basic sources and felsic island arc sources. In particular, the La/Sc versus Ti/Zr plot[81] suggests a predominantly continental island arc setting for the Middle Permian Lucaogou Formation (Figure 13d). This interpretation is also reinforced by the Sc−Th−Zr/10 and Co−Th−Zr/10 relationships[81] as

https://doi.org/10.1021/acsearthspacechem.2c00245
ACS Earth Space Chem. 2022, 6, 2530−2551

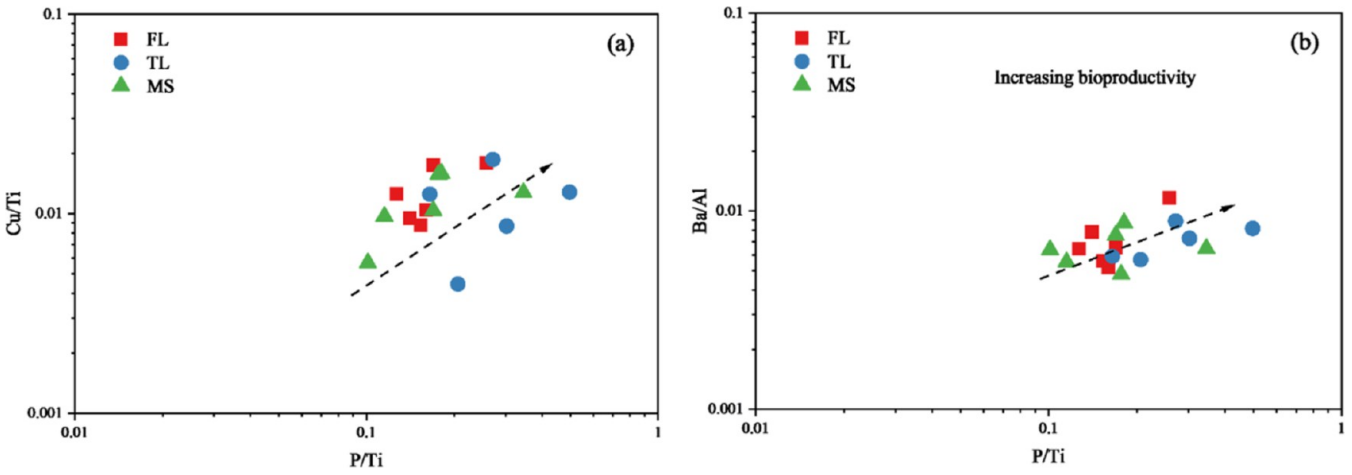

Figure 16. Paleoproductivity index of Lucaogou source rocks: (a) P/Ti versus Cu/Ti and (b) P/Ti versus Ba/Al.

most of the LCG source rocks are scattered in the continental island arc zone (Figure 13e,f).

5.2.2. Silica Origin and the Detrital Influx. During the exploitation of shale oil, high brittle mineral content often suggests good fractability, which leads to better exploration potential. For the mixed Lucaogou source rocks, quartz is one of the predominant brittle minerals. In general, terrigenous debris influx, hydrothermalism, and diagenesis are the three main quartz sources in shale.[82]

Generally, (Fe + Mn)/Ti > 15 and Fe/Ti > 20 indicate hydrothermal activities during sedimentation.[77] According to Table 5, the average (Fe + Mn)/Ti and Fe/Ti ratios range at 3.80−40.28 (average = 3.80) and 3.60−35.28 (average = 10.03), respectively, indicating that the Jimusar Sag experienced slight hydrothermal input during the Middle Permian. The Al/(Al + Fe + Mn) ratio is commonly used to distinguish silica sources in shales.[83,84] According to Adachi et al., the representative hydrothermal deposits are distinguished by Al/(Al + Mn + Fe) < 0.4[85] The Lucaogou source rock exhibit high Al/(Al + Fe + Mn) ratio values (0.48−0.83, average 0.67), suggesting that the possibility of silica from the hydrothermal activity is low. Furthermore, Lucaogou source rocks mainly fall in the nonhydrothermal region in the Al−Fe−Mn ternary diagram (Figure 14a), indicating the nonhydrothermal silica origin.

The terrigenous debris influx is another silica source. Elements Al, Ti, and Zr are good indicators of detrital influx.[34] To clarify the impact of the terrigenous debris influx, we charted the correlation between Si and elements Al, Zr, and Ti (Figure 14b−d). The apparent correlation between Si and Zr concentrations suggests an abiotic detrital source of silica, while a negative correlation implies a biogenic source for silica.[86] In our study, the Si−Zr scatter diagram shows that most samples are plotted on the detrital trend (Figure 14c), indicating that silica was derived primarily from a terrigenous input. Al, Zr, and Ti show a positive relationship with Si, indicating that Si is mainly sourced from aluminosilicate minerals (Figure 14b−d). The good Ti−Al relationship suggests that Ti is derived from the continual detrital material or clay lattices (Figure 14e).[63] The good correlation between Zr and Al (Figure 13f) perhaps suggests a relatively consistent detrital input.

Diagenesis also plays a non-negligible role in siliceous matter enrichment.[87] The relative content of excess silica (EX-SiO_2) is calculated by eq 4.

$$\mathrm{EX-SiO_2} = \mathrm{SiO_{2(sample)}} - (\mathrm{SiO_2/Al_2O_3})_{\text{average shale}} \times \mathrm{Al_2O_{3(sample)}} \quad (4)$$

where $(SiO_2/Al_2O_3)_{\text{average shale}}$ is the average ratio of SiO_2 to Al_2O_3.[34,88−90] According to the crossplot between the EX-SiO_2 content and paleoproductivity elements (Ni, Cu, and Zn), the EX-SiO_2 values in the TL shale show stable characteristics, while in the MS shale, the values show a positive increase (Figure 15), indicating that the silicate in massive shale is mixed with some biogenic silica origin. The presence of in situ quartz silt in MS shale suggests that the high surface productivity in MS shale also contributes to abundant OM accumulation.[2] In summary, for the majority of source rocks with fine and thick laminae, the Si content is mainly derived from the terrestrial debris influx except for some biogenic origin mixed in MS shale samples.

5.2.3. Palaeoproductivity. P and Cu elements are the applicable indices of paleoproductivity.[34] The uptake of P is associated with algae growth. Cu is commonly existing as organometallic ligands.[88] In this study, the element ratios P/Ti, Cu/Ti, P/Al, and Cu/Al are used to evaluate the paleoproductivity, and these element ratios exclude the effects of terrigenous clastic supply.[34] A higher ratio suggests a stronger paleoproducitivity.[60]

The Lucaogou source rocks show that the P/Ti ratio at 0.10−0.50 (average = 0.21) is modestly higher than that of PAAS (0.13),[55] suggesting relatively higher productivity. The Cu/Ti ratio of Lucaogou shale (0.004−0.019; average = 0.012) presents a positive relationship with the P/Ti ratio (Figure 16a). A similar positive correlation is observed between P/Ti and Ba/Al (Figure 16b). Overall, the crossplots of Cu/Ti versus P/Ti and Ba/Al versus P/Ti illustrate that the paleoproductivity of shale and mudstone presents weak heterogeneity (Figure 16a,b).

5.3. Shale Oil Potential and Implications for Regional Hydrocarbon Exploration. *5.3.1. Effect of Paleoenvironment on Petrology.* For Lucaogou source rock samples, the *C*-value displays a medium negative correlation with carbonate mineral content (Figure 17a), indicating that the humid climate might hinder the development of carbonate minerals. During the climate transfer from arid to humid, only the clay mineral content increases (Figure 17b). The shale brittleness index (BI) is a significant marker during hydraulic fracturing in shale intervals.[91] In general, high-brittleness shale layers contribute to

https://doi.org/10.1021/acsearthspacechem.2c00245
ACS Earth Space Chem. 2022, 6, 2530−2551

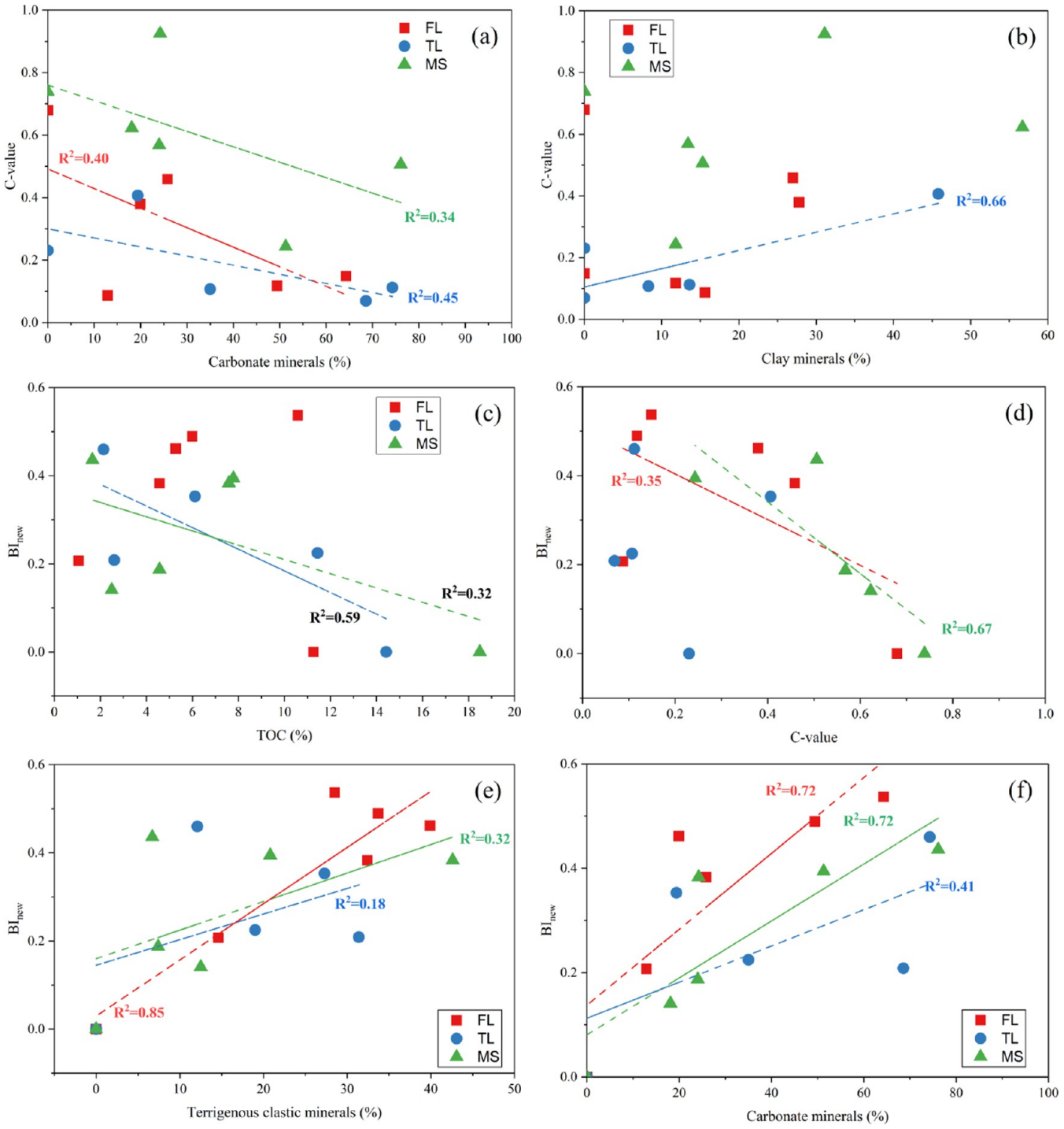

Figure 17. Correlation of paleoenvironment indices and the brittle index (BI_{new}): (a) carbonate minerals versus *C*-value, (b) clay mineral versus *C*-value, (c) TOC versus BI_{new}, (d) *C*-value versus BI_{new}, (e) terrigenous clastic minerals versus BI_{new}, and (f) carbonate minerals versus BI_{new}.

the increased porosity of the reservoir. The brittleness index (BI) can be calculated through the contents of brittle minerals. Kang et al. reported a new brittleness index considering both conventional brittle mineral contents and their mechanical heterogeneities.[92] Specifically, the four brittle minerals (quartz, feldspar, calcite, and dolomite) present different bulk moduli as 37.5, 76, 74, and 76−95, respectively.[93] Quartz is the most brittle mineral, and its bulk modulus is half of the other three brittle minerals. If a weighting coefficient 1 is arbitrarily assigned to quartz, then the weighting coefficients of feldspar, calcite, and dolomite are 0.49, 0.51, and 0.44, respectively.[92] The new brittleness index (BI_{new}) is expressed in eq 5

$$BI_{new} = (W_Q + W_F^*0.49 + W_C^*0.51 + W_D^*0.44)/W_T \quad (5)$$

where W_Q, W_F, W_C, and W_D are the weights of quartz, feldspar, calcite, and dolomite, respectively. W_T is the total mineral weight. To more clearly characterize the brittleness and its controlling factors, we quantified the brittleness following the new calculation proposed by Kang et al.[92] For MS shale, compared with terrigenous clastic minerals, carbonate minerals

https://doi.org/10.1021/acsearthspacechem.2c00245
ACS Earth Space Chem. 2022, 6, 2530−2551

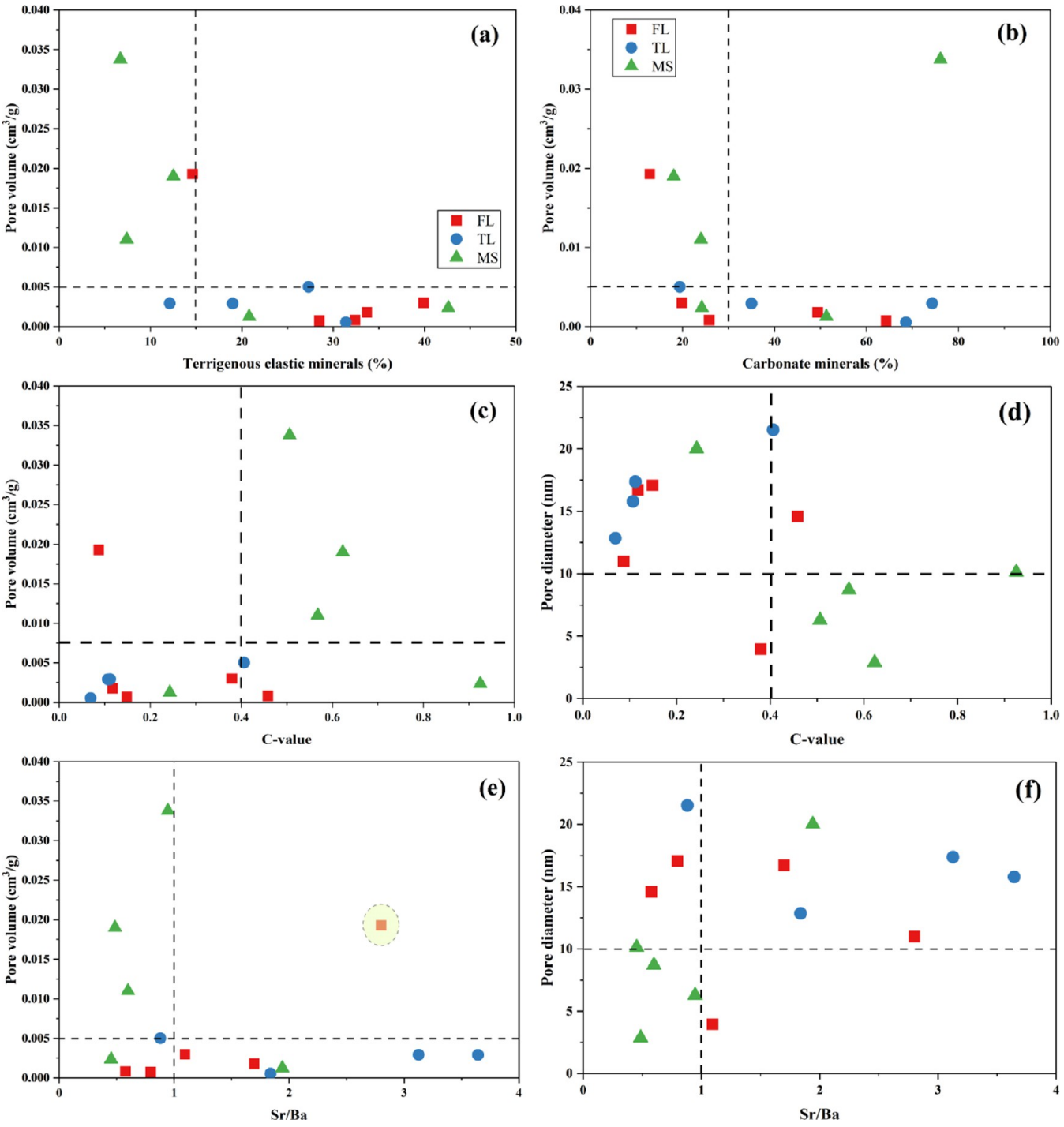

Figure 18. Correlation of paleoenvironment indices and pore structure parameters: (a) terrigenous clastic minerals versus pore volume, (b) carbonate minerals versus pore volume, (c) *C*-value versus pore volume, (d) *C*-value versus pore diameter, (e) Sr/Ba versus pore volume, and (f) Sr/Ba versus pore diameter.

present a higher positive correlation with the brittle index (Figure 17e,f), indicating that the fractability of MS shale is mainly controlled by carbonate minerals. However, both terrigenous clastic (R^2 = 0.85) and carbonate minerals (R^2 = 0.72) show a strong positive correlation with brittleness in FL shale samples (Figure 16a,b). Interestingly, the TL shale shows a medium-weak correlation between minerals and brittleness (Figure 17e,f), indicating that fractability might be controlled by other factors such as its thick laminae fabric and strong heterogeneity. The TOC content shows a medium negative effect on brittleness from both TL shale and MS shale (Figure 17c). Moreover, the negative correlation between the *C*-value and BI in FL and MS source rocks suggests that an arid and semiarid climate is beneficial to enhancing the fractability of FL and MS shales (Figure 17d).

5.3.2. Paleoenvironmental Indices and Their Influence on Pore Parameters. Compared with the typical alkaline Fengcheng Fm. from the Mahu Sag in the Santanghu Basin, the Lucaogou Fm. in the Junggar Basin might be deposited at the early stage of an alkaline lake.[42] For FL and MS shales, the

https://doi.org/10.1021/acsearthspacechem.2c00245
ACS Earth Space Chem. 2022, 6, 2530−2551

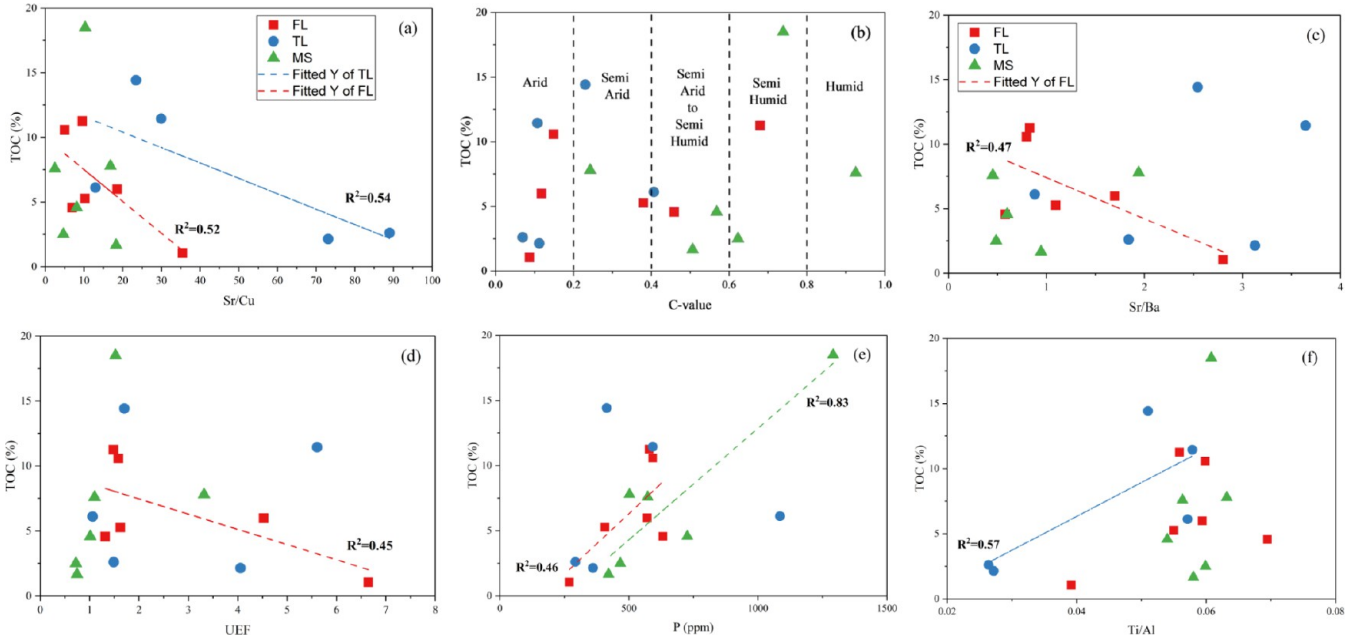

Figure 19. Correlation of paleoenvironment indices and TOC: (a) Sr/Cu versus TOC; (b) *C*-value versus TOC; (c) Sr/Ba versus TOC; (d) U_{EF} versus TOC; (e) P versus TOC; and (f) Ti/Al versus TOC: total organic carbon.

terrigenous clastic minerals present a medium-to-high negative correlation with total pore volume at the nanoscale (Figure 18a). A similar hinder effect is also observed in carbonate minerals for both FL and MS shales except for one outlier of a massive sample (Figure 18b). However, for the TL shale, the effect of minerals on pore volume is not apparent (Figure 18a,b). In addition, when the *C*-value is lower than 0.4, the pore volume in most of the Lucaogou source rocks is mainly lower than 0.01 cm^3/g, when the *C*-value > 0.4−0.5, the pore volume shows a sharp increase trend (Figure 18c), interestingly, the average pore diameter in a humid climate is much smaller than relatively arid climate (Figure 18d). The Lucaogou source rocks present a decreasing pore volume and increasing average diameter with increasing paleosalinity (Figure 18e,f).

5.3.3. Paleoenvironment on the Accumulation of Organic Matter. The accumulation of OM is greatly affected by paleoproductivity, paleoclimate, terrestrial influx, and paleoredox. The bioprecursor of the Middle Permian LCG Fm. in the Junggar Basin is mixed with aquatic bacteria, freshwater algae, and terrestrial higher plants.[42,69] The accumulation model could be further divided into preservation and productivity models.[60]Figure 19 shows the multiple relationships between some abovementioned indicators and TOC contents. Remarkably, TOC content exhibits a negative correlation with the Sr/Cu ratio, especially for the TL and FL shale source rocks (Figure 19a). This indicates that the warm and humid climate can support the organic matter accumulation in shale. This interpretation is consistent with previous studies.[60] Interestingly, the majority of MS shale samples are plotted in the humid climate zone with a lower Sr/Cu ratio and a higher *C*-value than FL and TL shales (Figure 19a,b). This denotes that the MS shale is mainly formed in a warm and humid climate. For the massive shale, there is no apparent linear correlation between TOC and the Sr/Cu ratio (Figure 19a), indicating that OM accumulation in massive shale is not controlled by paleoclimate (Figure 19a,b). The paleosalinity (Sr/Ba ratio) shows a medium negative correlation with FL shale and presents no obvious influence on OM accumulation in MS and TL source rocks (Figure 19c). This indicates that the effect of paleosalinity on OM accumulation is more important for FL shale. This is consistent with a former study on OM in the Eocene Youganwo Formation, Maoming Basin.[94] The redox (U_{EF}) proxies exhibit no linear correlation with TOC content in MS and TL source rocks (Figure 18d) and a medium negative relationship in FL shale samples (Figure 19d). The variation trends of the the paleoredox condition on TOC are approximately similar to those of paleosalinity (Figure 19c,d). All of these observations indicate that the single anoxic condition might play a limited role in controlling the accumulation of OM. Additionally, the paleoproductivity index (P content)) is positively correlated with TOC in diverse degrees in FL (R^2 = 0.46) and MS (R^2 = 0.83) source rocks (Figure 19e), indicating that paleoproductivity is conducive to OM accumulation in MS and FL shales. Interestingly, paleoproductivity presents a progressively positive impact on source rocks when the rock fabric transforms from thick laminae to massive. The terrigenous clastic influx (Ti/Al) displays no linear correlation with the TOC content for FL and MS shales (Figure 18f). However, terrigenous clast plays a medium positive role in OM enrichment in TL shale (Figure 19f). This suggests that the terrestrial influx during organic-rich laminae deposition is significant to OM enrichment in the TL shale.

The above analysis shows that lower salinity, humid climate, and strong terrigenous clastic input jointly enhance OM accumulation in FL and MS shales. It can be concluded that the warm and humid climate contributed to the blooming of lake algae and regeneration of terrestrial vegetation, and the intense paleo weathering conditions and abundant rainfall also led to the increase in the terrestrial nutrient input, which improved the lake bioproductivity and was positive to the accumulation of OM.

6. CONCLUSIONS

The Permian Lucaogou Formation in the Jimusar Sag deposits organic-rich laminated and massive shales formed in a salinized

https://doi.org/10.1021/acsearthspacechem.2c00245
ACS Earth Space Chem. 2022, 6, 2530−2551

paleolake. Their organic enrichment, lithological facies, pore structures, and sedimentary geochemical proxies were systematically compared. The main conclusions are as follows:

(1) Both laminated and massive shales are thermally mature and oil-prone and have high shale oil generation potential. The warm and humid climate is conducive to organic matter accumulation in shale. Paleoproductivity presents an increasingly positive impact on source rocks when the rock fabric transforms from massive to thick laminae.

(2) The Lucaogou source rocks are mainly derived from mixed felsic and basic sources and felsic island arc sources. They experienced slight hydrothermal input but a relatively greater terrigenous input. The laminated shale is mainly formed in a hot and dry climate with weak weathering and relatively higher salinity. However, the massive shale is mainly related to a warm and humid climate with moderate weathering and lower salinity conditions.

(3) Lower salinity, humid climate, and strong terrigenous clastic input jointly enhance OM accumulation in laminated and MS shales. The arid climate and the high content of carbonate minerals are beneficial to enhancing the fractability of FL and MS shales. The massive shale contains a higher pore volume and a smaller pore diameter than FL and TL shales. This character is controlled by its lower salinity and humid climate.

AUTHOR INFORMATION

Corresponding Authors

Jianhui Zeng − *State Key Laboratory of Petroleum Resources and Prospecting, China University of Petroleum (Beijing), Beijing 102249, China; College of Geosciences, China University of Petroleum (Beijing), Beijing 102249, China;* orcid.org/0000-0003-4768-043X; Email: zengjh@cup.edu.cn

Juncheng Qiao − *State Key Laboratory of Petroleum Resources and Prospecting, China University of Petroleum (Beijing), Beijing 102249, China; College of Geosciences, China University of Petroleum (Beijing), Beijing 102249, China*; Email: Juncheng.Qiao@cup.edu.cn

Authors

Guangqing Yang − *State Key Laboratory of Petroleum Resources and Prospecting, China University of Petroleum (Beijing), Beijing 102249, China; College of Geosciences, China University of Petroleum (Beijing), Beijing 102249, China*

Yazhou Liu − *State Key Laboratory of Petroleum Resources and Prospecting, China University of Petroleum (Beijing), Beijing 102249, China; College of Geosciences, China University of Petroleum (Beijing), Beijing 102249, China*

Weifu Cao − *Exploration and Development Research Institute, PetroChina Daqing Oilfield Company, Daqing 163712, China*

Chengyun Wang − *Exploration and Development Research Institute, PetroChina Huabei Oilfield Company, Renqiu 062552, China*

Feng Geng − *State Key Laboratory of Petroleum Resources and Prospecting, China University of Petroleum (Beijing), Beijing 102249, China; College of Geosciences, China University of Petroleum (Beijing), Beijing 102249, China*

Wenfei Wei − *State Key Laboratory of Petroleum Resources and Prospecting, China University of Petroleum (Beijing), Beijing 102249, China; College of Geosciences, China University of Petroleum (Beijing), Beijing 102249, China*

Complete contact information is available at: https://pubs.acs.org/10.1021/acsearthspacechem.2c00245

Notes

The authors declare no competing financial interest.

The authors declare that they have no known competing financial interests or personal relationships that could have appeared to influence the work reported in this paper.

ACKNOWLEDGMENTS

The authors sincerely thank the Experimental Center of Exploration and Development Research Institute of PetroChina Xinjiang Oilfield Company for their convenience in data and sample collection. This work was financially supported by the National Natural Science Foundation of China (Grant No. 41972147).

REFERENCES

(1) MacQuaker, J. H. S.; Adams, A. E. Maximizing information from fine-grained sedimentary rocks: An inclusive nomenclature for mudstones. *J. Sediment. Res.* **2003**, *73*, 735−744.

(2) Schieber, J.; Krinsley, D.; Riciputi, L. Diagenetic origin quartz silt in mudstones and implications for silica cycling. *Nature* **2000**, *406*, 981−985.

(3) Shanmugam, G. The Bouma sequence and the turbidite mind set. *Earth-Sci. Rev.* **1997**, *42*, 201−229.

(4) Sharma, S.; Agrawal, V.; Akondi, R. N. Role of biogeochemistry in efficient shale oil and gas production. *Fuel* **2020**, *259*, No. 116207.

(5) Xin, B.; Zhao, X.; Hao, F.; Jin, F.; Pu, X.; Han, W.; Xu, Q.; Guo, P.; Tian, J. Laminae Characteristics of Lacustrine Shales from the Paleogene Kongdian Formation in the Cangdong Sag, Bohai Bay Basin, China: Why Do Laminated Shales Have Better Reservoir Physical Properties? *Int. J. Coal Geol.* **2022**, *260*, No. 104056.

(6) Li, T.; Jiang, Z.; Su, P.; Zhang, X.; Chen, W.; Wang, X.; Ning, C.; Wang, Z.; Xue, Z. Effect of laminae development on pore structure in the lower third member of the Shahejie Shale, Zhanhua Sag, Eastern China. *Interpretation* **2020**, *8*, T103−T114.

(7) Li, Y.; Pan, S.; Ning, S.; Shao, L.; Jing, Z.; Wang, Z. Coal measure metallogeny: Metallogenic system and implication for resource and environment. *Sci. China: Earth Sci.* **2022**, *65*, 1211−1228.

(8) Li, Y.; Chen, J.; Yang, J.; Liu, J.; Tong, W. Determination of shale macroscale modulus based on microscale measurement: A case study concerning multiscale mechanical characteristics. *Pet. Sci.* **2022**, *19*, 1262−1275.

(9) Shi, J.; Jin, Z.; Liu, Q.; Zhang, T.; Fan, T.; Gao, Z. Laminar characteristics of lacustrine organic-rich shales and their significance for shale reservoir formation: A case study of the Paleogene shales in the Dongying Sag, Bohai Bay Basin, China. *J. Asian Earth Sci.* **2022**, *223*, No. 104976.

(10) Wang, L.; Yang, H.; Guo, Y.; Bi, Z.; Guo, W.; Yang, C. Comparative Study of Marine and Lacustrine Shale Reservoirs from the Viewpoint of Rock Mechanics. *Energy Fuels* **2021**, *35*, 19481−19495.

(11) Li, Y.; Wang, Z.; Pan, Z.; Niu, X.; Yu, Y.; Meng, S. Pore structure and its fractal dimensions of transitional shale: A cross-section from east margin of the Ordos Basin, China. *Fuel* **2019**, *241*, 417−431.

(12) Mills, N. T.; Reece, J. S.; Tice, M. M. Clay minerals modulate early carbonate diagenesis. *Geology* **2021**, *49*, 1015−1019.

(13) Cao, Z.; Jiang, H.; Zeng, J.; Saibi, H.; Lu, T.; Xie, X.; Zhang, Y.; Zhou, G.; Wu, K.; Guo, J. Nanoscale liquid hydrocarbon adsorption on clay minerals: A molecular dynamics simulation of shale oils. *Chem. Eng. J.* **2021**, *420*, 1−12.

(14) Rahman, H. M.; Kennedy, M.; Löhr, S.; Dewhurst, D. N.; Sherwood, N.; Yang, S.; Horsfield, B. The influence of shale depositional fabric on the kinetics of hydrocarbon generation through

control of mineral surface contact area on clay catalysis. *Geochim. Cosmochim. Acta* **2018**, *220*, 429−448.
(15) Lewan, M. D. Laboratory classification of very fine grained sedimentary rocks. *Geology* **1978**, *6*, 745−748.
(16) Slatt, R. M.; Brien, N. R. O. Pore types in the Barnett and Woodford gas shales: Contribution to understanding gas storage and migration pathways in fine-grained rocks. *Am. Assoc. Pet. Geol. Bull.* **2017**, *12*, 2017−2030.
(17) Hildenbrand, A.; Schlo, S.; Kohle, D.; Spa, E.; Milanese, S. D. Gas breakthrough experiments on fine-grained sedimentary rocks. *Geofluids* **2002**, *2*, 3−23.
(18) Mount, J. F. Mixing of siliciclastic and carbonate sediments in shallow shelf environments. *Geology* **1984**, *12*, 432−435.
(19) Liu, Z.; Zhang, Y.; Song, G.; Li, S.; Long, G.; Zhao, J.; Zhu, C.; Wang, Y.; Gong, Q.; Xia, Z. Mixed carbonate rocks lithofacies features and reservoirs controlling mechanisms in a saline lacustrine basin in Yingxi area, Qaidam Basin, NW China. *Pet. Explor. Dev.* **2021**, *48*, 80−94.
(20) Pan, Y.; Huang, Z.; Li, T.; Xu, X.; Chen, X.; Guo, X. Pore structure characteristics and evaluation of lacustrine mixed fine-grained sedimentary rocks: A case study of the Lucaogou Formation in the Malang Sag, Santanghu Basin, Western China. *J. Pet. Sci. Eng.* **2021**, *201*, No. 108545.
(21) Xu, Q.; Hao, F.; Ma, Y.; Liu, B.; Song, X. Effects of the matrix on the oil production of supertight limestone in a lacustrine mixed sedimentary environment: The case of the Jurassic Da'anzhai member in the central Sichuan Basin, China. *Mar. Pet. Geol.* **2020**, *121*, No. 104583.
(22) Ye, M.; Xie, X.; Swennen, R.; Xu, C.; Du, X.; Du, X. Depositional characteristics of a lacustrine mixed sediment system: A case study from the eastern Shijiutuo Uplift, offshore Bohai Bay Basin, eastern China. *J. Asian Earth Sci.* **2021**, *209*, No. 104671.
(23) Zhang, S.; Cao, Y.; Liu, K.; Jahren, J.; Xi, K.; Zhu, R.; Yang, T.; Cao, X.; Wang, W. Characterization of lacustrine mixed fine-grained sedimentary rocks using coupled chemostratigraphic-petrographic analysis: A case study from a tight oil reservoir in the Jimusar Sag, Junggar Basin. *Mar. Pet. Geol.* **2019**, *99*, 453−472.
(24) Zhu, H.; Zeng, Z.; Xie, X.; Zhu, X.; Xu, C.; Zeng, H. Introduction to special section: Mapping mixed clastic and carbonate depositional systems in lacustrine basins. *Interpretation* **2021**, *9*, No. Sci.
(25) Wei, W.; Azmy, K.; Zhu, X. Impact of diagenesis on reservoir quality of the lacustrine mixed carbonate-siliciclastic-volcaniclastic rocks in China. *J. Asian Earth Sci.* **2022**, *233*, No. 105265.
(26) Gao, Y.; Huang, H.; Tao, H.; Carroll, A. R.; Qin, J.; Chen, J.; Yuan, X.; Wang, C. Paleoenvironmental setting, mechanism and consequence of massive organic carbon burial in the Permian Junggar Basin, NW China. *J. Asian Earth Sci.* **2020**, *194*, No. 104222.
(27) Xu, Z.; Wang, Y.; Jiang, S.; Fang, C.; Liu, L.; Wu, K.; Luo, Q.; Li, X.; Chen, Y. Impact of input, preservation and dilution on organic matter enrichment in lacustrine rift basin: A case study of lacustrine shale in Dehui Depression of Songliao Basin, NE China. *Mar. Petr. Geol.* **2022**, *135*, No. 105386.
(28) Fan, X.; Wang, G.; Li, Y.; Dai, Q.; Linghu, S.; Duan, C.; Zhang, C.; Zhang, F. Pore structure evaluation of tight reservoirs in the mixed siliciclastic-carbonate sediments using fractal analysis of NMR experiments and logs. *Mar. Pet. Geol.* **2019**, *109*, 484−493.
(29) Zhang, J.; Liu, G.; Cao, Z.; Tao, S.; Felix, M.; Kong, Y.; Zhang, Y. Characteristics and formation mechanism of multi-source mixed sedimentary rocks in a saline lake, a case study of the Permian Lucaogou Formation in the Jimusaer Sag, Northwest China. *Mar. Pet. Geol.* **2019**, *102*, 704−724.
(30) Huang, H.; Gao, Y.; Jones, M. M.; Tao, H.; Carroll, A. R.; Ibarra, D. E.; Wu, H.; Wang, C. Astronomical forcing of Middle Permian terrestrial climate recorded in a large paleolake in northwestern China. *Palaeogeogr., Palaeoclimatol., Palaeoecol.* **2020**, *550*, No. 109735.
(31) Cao, Z.; Liu, G.; Zhan, H.; Gao, J.; Zhang, J.; Li, C.; Xiang, B. Geological roles of the siltstones in tight oil play. *Mar. Pet. Geol.* **2017**, *83*, 333−344.
(32) Ding, X.; Gao, C.; Zha, M.; Chen, H.; Su, Y. Depositional environment and factors controlling β-Carotane accumulation: A case study from the Jimsar Sag, Junggar Basin, northwestern China. *Palaeogeogr., Palaeoclimatol., Palaeoecol.* **2017**, *485*, 833−842.
(33) Wang, E.; Guo, T.; Li, M.; Li, C.; Dong, X.; Zhang, N.; Feng, Y. Exploration potential of different lithofacies of deep marine shale gas systems: Insight into organic matter accumulation and pore formation mechanisms. *J. Nat. Gas Sci. Eng.* **2022**, *102*, No. 104563.
(34) Tribovillard, N.; Algeo, T. J.; Lyons, T.; Riboulleau, A. Trace metals as paleoredox and paleoproductivity proxies: An update. *Chem. Geol.* **2006**, *232*, 12−32.
(35) Tan, J.; Wang, Z.; Wang, W.; Hilton, J.; Guo, J.; Wang, X. Depositional environment and hydrothermal controls on organic matter enrichment in the lower Cambrian Niutitang Shale, southern China. *Am. Assoc. Pet. Geol. Bull.* **2021**, *105*, 1329−1356.
(36) Algeo, T. J.; Liu, J. A re-assessment of elemental proxies for paleoredox analysis. *Chem. Geol.* **2020**, *540*, No. 119549.
(37) Bennett, W. W.; Canfield, D. E. Redox-sensitive trace metals as paleoredox proxies: A review and analysis of data from modern sediments. *Earth-Sci. Rev.* **2020**, *204*, No. 103175.
(38) Charreau, J.; Kent-Corson, M. L.; Barrier, L.; Augier, R.; Ritts, B. D.; Chen, Y.; France-Lannord, C.; Guilmette, C. High-resolution stable isotopic record from the Junggar Basin (NW China): Implications for the paleotopographic evolution of the Tianshan mountains. *Earth Planet. Sci. Lett.* **2012**, *341*−*344*, 158−169.
(39) (a) Cao, Z.; Liu, G.; Kong, Y.; Wang, C.; Niu, Z.; Zhang, J.; Geng, C.; Shan, X.; Wei, Z. Lacustrine tight oil accumulation characteristics: Permian Lucaogou Formation in Jimusaer Sag, Junggar Basin. *Int. J. Coal Geol.* **2016**, *153*, 37−51. (b) Liu, Y.; Zeng, J.; Yang, G.; Jia, W.; Liu, S.; Kong, X.; Li, S. An innovative method for the characterization of oil content in lacustrine shale-oil systems: A case study from the Middle Permian Lucaogou Formation in the Jimusaer Sag, Junggar Basin. *Mar. Pet. Geol.* **2021**, *130*, No. 105112.
(40) Luo, X.; Wang, Z.; Zhang, L.; Yang, W.; Liu, L. Overpressure generation and evolution in a compressional tectonic setting, the margin of Junggar Basin, Northwestern China. *Am. Assoc. Pet. Geol. Bull.* **2007**, *91*, 1123−1139.
(41) Carroll, A. R.; Wartes, M. A. In *Organic carbon burial by large Permian lakes, Northwest China*, Special Papers-Geological Society of America, 2003; pp 91−104.
(42) Xia, L.; Cao, J.; Hu, W.; Zhi, D.; Tang, Y.; Li, E.; He, W. Coupling of paleoenvironment and biogeochemistry of deep-time alkaline lakes: A lipid biomarker perspective. *Earth-Sci. Rev.* **2021**, *213*, No. 103499.
(43) Mendonça, R.; Müller, R. A.; Clow, D.; Verpoorter, C.; Raymond, P.; Tranvik, L. J.; Sobek, S. Organic carbon burial in global lakes and reservoirs. *Nat. Commun.* **2017**, *8*, No. 1694.
(44) Li, Y.; Wang, Z.; Gan, Q.; Niu, X.; Xu, W. Paleoenvironmental conditions and organic matter accumulation in upper Paleozoic organic-rich rocks in the east margin of the Ordos Basin, China. *Fuel* **2019**, *252*, 172−187.
(45) Jarvie, D. M.; Hill, R. J.; Ruble, T. E.; Pollastro, R. M.; Jarvie, D. M.; Geochemical, H. Unconventional shale-gas systems: The Mississippian Barnett Shale of North-Central Texas as one model for thermogenic shale-gas assessment. *AAPG Bull.* **2007**, *91*, 475−499.
(46) Jarvie, D. M. Shale resource systems for oil and gas: Part 2—Shale-oil resource systems. *AAPG Mem.* **2012**, *97*, 89−119.
(47) Li, Y.; Zhang, C.; Tang, D.; Gan, Q.; Niu, X.; Wang, K.; Shen, R. Coal pore size distributions controlled by the coalification process: An experimental study of coals from the Junggar, Ordos and Qinshui basins in China. *Fuel* **2017**, *206*, 352−363.
(48) Li, Y.; Chen, J.; Elsworth, D.; Pan, Z.; Ma, X. Nanoscale mechanical property variations concerning mineral composition and contact of marine shale. *Geosci. Front.* **2022**, *13*, No. 101405.
(49) Sing, K. S. W.; Everett, D. H.; Haul, R. A. W.; Moscou, L.; Pierotti, R. A.; Rouquerol, J.; Siemieniewska, T. Reporting hysisorption data for gas/solid systems—with special reference to the determination of surface area and porosity. *Pure Appl. Chem.* **1985**, *57*, 603−619.
(50) Thommes, M.; Kaneko, K.; Neimark, A. V.; Olivier, J. P.; Rodriguez-Reinoso, F.; Rouquerol, J.; Sing, K. S. W. Physisorption of

gases, with special reference to the evaluation of surface area and pore size distribution (IUPAC technical report). *Pure Appl. Chem.* **2015**, *87*, 1051−1069.
(51) Peters, K. E. Guidelines for evaluating petroleum source rock using programmed pyrolysis. *Am. Assoc. Pet. Geol. Bull.* **1986**, *70*, 318−329.
(52) Langford, F. F.; Blanc-Valleron, M.-M. Interpreting Rock-Eval pyrolysis data using graphs of pyrolizable hydrocarbons vs. Total organic carbon. *Am. Assoc. Pet. Geol. Bull.* **1990**, *74*, 799−804.
(53) Peters, K. E.; Cassa, M. R. Applied source rock geochemistry. *AAPG Mem.* **1994**, 93−120.
(54) Chen, X.; Qu, X.; Xu, S.; Wang, W.; Li, S.; He, H.; Liu, Y. Dissolution pores in shale and their influence on reservoir quality in Damintun depression, Bohai Bay Basin, East China: Insights from SEM images, N_2 adsorption and fluid-rock interaction experiments. *Mar. Pet. Geol.* **2020**, *117*, No. 104394.
(55) Taylor, S. R.; McLennan, S. M.*The Continental Crust: Its Composition and Evolution*; Blackwell: Oxford, 1985, p 312.
(56) Berger, A.; Janots, E.; Gnos, E.; Frei, R.; Bernier, F. Rare earth element mineralogy and geochemistry in a laterite profile from Madagascar. *Appl. Geochem.* **2014**, *41*, 218−228.
(57) Tao, S.; Tang, D.; Xu, H.; Liang, J.; Shi, X. Organic geochemistry and elements distribution in Dahuangshan oil shale, southern Junggar Basin: Origin of organic matter and depositional environment. *Int. J. Coal Geol.* **2013**, *115*, 41−51.
(58) Liu, D.; Kong, X.; Zhang, C.; Wang, J.; Yang, D.; Liu, X.; Wang, X.; Song, Y. Provenance and geochemistry of lower to middle Permian strata in the southern Junggar and Turpan Basins: A terrestrial record from Mid-Latitude NE Pangea. *Palaeogeogr., Palaeoclimatol., Palaeoecol.* **2018**, *495*, 259−277.
(59) Nesbitt, H. W.; Young, G. M. Early Proterozoic climates and plate motions inferred from major element chemistry of lutites. *Nature* **1982**, *299*, 715−717.
(60) Wu, Z.; Zhao, X.; Wang, E.; Pu, X.; Lash, G.; Han, W.; Zhang, W.; Feng, Y. Sedimentary environment and organic enrichment mechanisms of lacustrine shale: A case study of the Paleogene Shahejie Formation, Qikou Sag, Bohai Bay Basin. *Palaeogeogr., Palaeoclimatol., Palaeoecol.* **2021**, *573*, No. 110404.
(61) McLennan, S. M.; Hemming, S.; McDaniel, D. K.; Hanson, G. N. In *Geochemical Approaches to Sedimentation, Provenance, and Tectonics*, Special Papers-Geological Society of America, 1993; pp 21−40.
(62) Kasanzu, C.; Maboko, M. A. H.; Manya, S. Geochemistry of fine-grained clastic sedimentary rocks of the Neoproterozoic Ikorongo Group, NE Tanzania: Implications for provenance and source rock weathering. *Precambrian Res.* **2008**, *164*, 201−213.
(63) Zhang, L.; Dong, D.; Qiu, Z.; Wu, C.; Zhang, Q.; Wang, Y.; Liu, D.; Deng, Z.; Zhou, S.; Pan, S. Sedimentology and geochemistry of Carboniferous-Permian marine-continental transitional shales in the eastern Ordos Basin, North China. *Palaeogeogr., Palaeoclimatol., Palaeoecol.* **2021**, *571*, No. 110389.
(64) Sarki Yandoka, B. M.; Abdullah, W. H.; Abubakar, M. B.; Hakimi, M. H.; Adegoke, A. K. Geochemical characterisation of early Cretaceous lacustrine sediments of Bima Formation, Yola Sub-Basin, Northern Benue Trough, NE Nigeria: Organic matter input, preservation, paleoenvironment and palaeoclimatic conditions. *Mar. Pet. Geol.* **2015**, *61*, 82−94.
(65) Cao, J.; Wu, M.; Chen, Y.; Hu, K.; Bian, L.; Wang, L.; Zhang, Y. Trace and rare earth element geochemistry of Jurassic mudstones in the northern Qaidam Basin, Northwest China. *Geochemistry* **2012**, *72*, 245−252.
(66) Tao, S.; Xu, Y.; Tang, D.; Xu, H.; Li, S.; Chen, S.; Liu, W.; Cui, Y.; Gou, M. Geochemistry of the Shitoumei oil shale in the Santanghu Basin, Northwest China: Implications for paleoclimate conditions, weathering, provenance and tectonic setting. *Int. J. Coal Geol.* **2017**, *184*, 42−56.
(67) Ding, Z. L.; Sun, J. M.; Yang, S. L.; Liu, T. S. Geochemistry of the Pliocene Red Clay Formation in the Chinese Loess Plateau and implication for its origin, source provenance and paleoclimate change. *Geochim. Cosmochim. Acta* **2001**, *65*, 901−913.
(68) Wei, W.; Algeo, T. J. Elemental proxies for paleosalinity analysis of ancient shales and mudrocks. *Geochim. Cosmochim. Acta* **2020**, *287*, 341−366.
(69) Cao, J.; Xia, L.; Wang, T.; Zhi, D.; Tang, Y.; Li, W. An alkaline lake in the Late Paleozoic Ice Age (LPIA): A review and new insights into paleoenvironment and petroleum geology. *Earth-Sci. Rev.* **2020**, *202*, No. 103091.
(70) Nothdurft, L. D.; Webb, G. E.; Kamber, B. S. Rare earth element geochemistry of late Devonian Reefal Carbonates, Canning Basin, western Australia: Confirmation of a seawater REE proxy in ancient limestones. *Geochim. Cosmochim. Acta* **2004**, *68*, 263−283.
(71) van Bentum, E. C.; Reichart, G. J.; Sinninghe Damsté, J. S. Organic matter provenance, palaeoproductivity and bottom water anoxia during the Cenomanian/Turonian cceanic anoxic event in the Newfoundland Basin (Northern Proto North Atlantic Ocean). *Org. Geochem.* **2012**, *50*, 11−18.
(72) Algeo, T. J.; Li, C. Redox classification and calibration of redox thresholds in sedimentary systems. *Geochim. Cosmochim. Acta* **2020**, *287*, 8−26.
(73) Tribovillard, N.; Algeo, T. J.; Baudin, F.; Riboulleau. Analysis of marine environmental conditions based on molybdenum-Uranium covariation-applications to Mesozoic paleoceanography. *Chem. Geol.* **2012**, *324*−*325*, 46−58.
(74) Algeo, T. J.; Ingall, E. Sedimentary Corg:P ratios, paleocean ventilation, and Phanerozoic atmospheric PO_2. *Palaeogeogr., Palaeoclimatol., Palaeoecol.* **2007**, *256*, 130−155.
(75) Calvert, S. E.; Bustin, R. M.; Ingall, E. D. Influence of water column anoxia and sediment supply on the burial and preservation of organic carbon in marine shales. *Geochim. Cosmochim. Acta* **1996**, *60*, 1577−1593.
(76) Tao, H.; Qiu, Z.; Qu, Y.; Liu, J.; Qin, Z.; Xie, Z.; Qiu, J.; Liu, B. Geochemistry of Middle Permian lacustrine shales in the Jimusar Sag, Junggar Basin, NW China: Implications for hydrothermal activity and organic matter enrichment. *J. Asian Earth Sci.* **2022**, *232*, No. 105267.
(77) He, C.; Ji, L.; Wu, Y.; Su, A.; Zhang, M. Characteristics of hydrothermal sedimentation process in the Yanchang Formation, south Ordos Basin, China: Evidence from element geochemistry. *Sediment. Geol.* **2016**, *345*, 33−41.
(78) Hayashi, K. I.; Fujisawa, H.; Holland, H. D.; Ohmoto, H. Geochemistry of ∼1.9 Ga sedimentary rocks from northeastern Labrador, Canada. *Geochim. Cosmochim. Acta* **1997**, *61*, 4115−4137.
(79) Floyd, P. A.; Leveridge, B. E. Tectonic environment of the Devonian Gramscatho Basin, south Cornwall: Framework mode and geochemical evidence from turbiditic sandstones. *J. Geol. Soc.* **1987**, *144*, 531−542.
(80) Soomer, S.; Somelar, P.; Mänd, K.; Lepland, A.; Kirsimäe, K. Geochemistry and mineralogy of Paleoproterozoic Metasediments in the Imandra-Varzuga Greenstone Belt: Implications for sediment provenance, tectonic settings and weathering intensity at the transition to oxygenated surface environments. *Precambrian Res.* **2022**, *371*, No. 106578.
(81) Bhatia, M. R.; Crook, K. A. W. Trace element characteristics of graywackes and tectonic setting discrimination of sedimentary basins. *Contrib. Mineral. Petrol.* **1986**, *92*, 181−193.
(82) Zhang, L.; Xiao, D.; Lu, S.; Jiang, S.; Lu, S. Effect of sedimentary environment on the formation of organic-rich marine shale: Insights from major/trace elements and shale composition. *Int. J. Coal Geol.* **2019**, *204*, 34−50.
(83) Tan, J.; Liu, J.; Kang, X.; Zhao, H.; Ma, Z.; Luo, W.; Schulz, H. M.; Shahzad, A.; Jan, I. U. Experimental gas generation of organic-rich shales at different oil expulsion efficiencies: Implications for shale gas evaluation. *Energy Fuels* **2021**, *35*, 5925−5940.
(84) Yamamoto, K. Geochemical characteristics and depositional environments of cherts and associated rocks in the Franciscan and Shimanto terranes. *Sediment. Geol.* **1987**, *52*, 65−108.
(85) Adachi, M.; Yamamoto, K.; Sugisaki, R. Hydrothermal chert and associated siliceous rocks from the northern Pacific: Their geological significance as indication of ocean ridge activity. *Sediment. Geol.* **1986**, *47*, 125−148.

https://doi.org/10.1021/acsearthspacechem.2c00245
ACS Earth Space Chem. 2022, 6, 2530−2551

(86) Wright, A. M.; Spain, D.; Ratcliffe, K. T. In *Application of Inorganic Whole Rock Geochemistry to Shale Resource Plays*, Canadian Unconventional Resources and International Petroleum Conference; OnePetro, 2010; pp 2473−2490.
(87) Li, D.; Li, R.; Tan, C.; Zhao, D.; Xue, T.; Zhao, B.; Khaled, A.; Liu, F.; Xu, F. Origin of silica, paleoenvironment, and organic matter enrichment in the lower Paleozoic Niutitang and Longmaxi Formations of the northwestern Upper Yangtze Plate: Significance for hydrocarbon exploration. *Mar. Pet. Geol.* **2019**, *103*, 404−421.
(88) Algeo, T. J. 1-Can marine anoxic events draw down the trace element inventory of seawater? *Geology* **2004**, *32*, 1057−1060.
(89) Calvert, S. E.; Pedersen, T. F. Geochemistry of Recent oxic and anoxic marine sediments: Implications for the geological record. *Mar. Geol.* **1993**, *113*, 67−88.
(90) Wedepohl, K. H. Environmental influences on the chemical composition of shales and clays. *Phys. Chem. Earth* **1971**, *8*, 305−333.
(91) Liu, B.; Wang, H.; Fu, X.; Bai, Y.; Bai, L.; Jia, M.; He, B. Lithofacies and depositional setting of a highly prospective lacustrine shale oil succession from the Upper Cretaceous Qingshankou Formation in the Gulong sag, northern Songliao Basin, northeast China. *AAPG Bull.* **2019**, *103*, 405−432.
(92) Kang, Y.; Shang, C.; Zhou, H.; Huang, Y.; Zhao, Q.; Deng, Z.; Wang, H.; Ma, Y. Z. Mineralogical brittleness index as a function of weighting brittle minerals—from laboratory tests to case study. *J. Nat. Gas Sci. Eng.* **2020**, *77*, No. 103278.
(93) Fjær, E.; Holt, R. M.; Horsrud, P.; Raaen, A. M.; Risnes, R.*Petroleum Related Rock Mechanics*, 2nd ed.; Elsevier, 2008.
(94) Xu, C.; Hu, F.; Meng, Q.; Liu, Z.; Shan, X.; Zeng, W.; Zhang, K.; He, W. Organic matter accumulation in the Youganwo Formation (Middle Eocene), Maoming Basin, South China: constraints from multiple geochemical proxies and organic petrology. *ACS Earth Space Chem.* **2022**, *6*, 714−732.

https://doi.org/10.1021/acsearthspacechem.2c00245
ACS Earth Space Chem. 2022, 6, 2530−2551